AIAA 2003-0922

RECOMMENDED EXPERIMENTAL PROCEDURES FOR EVALUATION OF ABRUPT WING STALL CHARACTERISTICS

F. J. Capone, R. M. Hall, D. B. Owens,
J. E. Lamar and S. N. McMillin
NASA Langley Research Center
Hampton, Virginia

41st AIAA Aerospace Sciences Meeting and Exhibit

6-9 January 2003
Reno, Nevada

AIAA-2003-0922

Recommended Experimental Procedures For Evaluation Of Abrupt Wing Stall Characteristics

F. J. Capone†, R. M. Hall*, D. B. Owens§,
J. E. Lamar‡, and S. N. McMillin**
NASA Langley Research Center, Hampton, Virginia

ABSTRACT

This paper presents a review of the experimental program under the Abrupt Wing Stall (AWS) Program. Candidate figures of merit from conventional static tunnel tests are summarized and correlated with data obtained in unique free-to-roll tests. Where possible, free-to-roll results are also correlated with flight data. Based on extensive studies of static experimental figures of merit in the Abrupt Wing Stall Program for four different aircraft configurations, no one specific figure of merit consistently flagged a warning of potential lateral activity when actual activity was seen to occur in the free-to-roll experiments. However, these studies pointed out the importance of measuring and recording the root mean square signals of the force balance.

SYMBOLS AND ABBREVIATIONS

AFOM	alternate figure of merit
AWS	abrupt wing stall
C_A	axial force coefficient
C_L	lift coefficient
$C_{L\alpha}$	lift-curve slope, per degree
C_l	rolling-moment coefficient
$C_{l,rms}$	root mean square of C_l
C_N	normal-force coefficient
$C_{N,rms}$	root mean square of C_N
C_m	pitching-moment coefficient
C_n	yawing-moment coefficient
C_{LWB}	left-wing bending-moment coefficient
$C_{LWB,rms}$	root mean square of C_{LWB}
C_{RWB}	right-wing bending-moment coefficient
$C_{RWB,rms}$	root mean square of C_{RWB}
C_Y	side-force coefficient
FOM	figure of merit
FTR	free-to-roll
LERX	leading-edge root extension
M	Mach number
RMS	root mean square
TFOM	traditional figure of merit
t	time
α	angle of attack, deg
δ_a	aileron angle, deg
δ_{le}	leading-edge flap angle, deg
δ_{te}	trailing-edge flap angle, deg
ϕ	model roll angle, deg
θ	model pitch angle, deg
ΣFOM,3	summation figure of merit (ref. 9)
ΣFOM,22	summation figure of merit (ref. 9)
πFOM	product figure of merit (ref. 9)
16-ft TT	16-Foot Transonic Tunnel

INTRODUCTION

A joint NASA/Navy/Air Force Abrupt Wing Stall Program (AWS) was established after several pre-production F/A-18E/F aircraft experienced severe wing-drop motions during the development stage. A Blue Ribbon Panel determined that a poor understanding of the phenomena causing the problem existed, and made the recommendation to: “Initiate a national research effort to thoroughly and systematically

†Senior Research Engineer,
*Senior Research Engineer, Associate Fellow AIAA
§ Aerospace Engineer, Member AIAA
‡ Aerospace Engineer, Member AIAA
**Senior Research Engineer, Associate Fellow AIAA

study the wing drop phenomena." The problem area addressed by the AWS Program[1-17] is the unexpected occurrence of highly undesirable lateral-directional motions at high-subsonic and transonic maneuvering conditions. One of the recommendations made by Chambers[2] was "to define and assess candidate figures of merit for the prediction of wing drop and wing rock from experimental methods."

The interpretation of experimental data obtained in wind tunnels for conditions involving highly separated wing flows has always been very subjective and open to many opinions as to what is happening. One aircraft that went through an extensive experimental program because of uncommanded wing rock/drop was the Harrier[18]. The potential existence of wing rock/drop was interpreted from wind-tunnel rolling-moment data recorded with on-line continuous pen recorders as shown in figure 1. For example, a continuous oscillation of the pen was interpreted to be wing rock, whereas a steady departure was considered to be wing drop. Note the relatively smooth lift curves with no abrupt breaks.

This paper will review the scope of the experimental program conducted under the Abrupt Wing Stall (AWS) Program. Four different aircraft configurations that either do or do not exhibit uncommanded lateral motions were tested. Along with the pre-production F/A-18E, the AV-8B was chosen as a configuration that exhibits wing drop. The two configurations that do not have wing-drop were the F/A-18C and the F-16C. Candidate figures of merit from conventional static tunnel tests are summarized and correlated with data obtained in unique free-to-roll tests. Where possible, free-to-roll results are also correlated with flight data. Recommendations as to how to conduct an experimental program on future vehicles are made.

In order to obtain approval for releasing this paper to the public, quantitative information has been removed from most vertical scales as per guidelines from the Department of Defense.

ABRUPT WING STALL EXPERIMENTAL PROGRAM

An extensive experimental wind-tunnel test program has been conducted as part of the AWS program. Early in the AWS program[1], a series of tests were conducted on an 8-percent pre-production F/A-18E model with new set of wings that were heavily instrumented with wing bending-moment gauges, static-pressure taps, and unsteady pressure gauges. Both static and dynamic force balance measurements were made, as well a tunnel entry devoted to using the pressure sensitive paint technique[3,5]. These tests were conducted prior to the operational readiness of the free-to-roll rig[10].

One of the objectives of the AWS program was to test four different aircraft that are known to either exhibit uncommanded lateral motions or not. Along with the pre-production F/A-18E, the AV-8B was chosen because it exhibited wing drop behavior. The two configurations that did not have wing-drop were the F/A-18C and the F-16C. The overall geometric dimensions of these models are also shown in figure 2 as well as a summary of the scope of experimental measurements made in the program.

All four models were tested in the 16-Foot Transonic Tunnel over an eleven-week period, during which both static and free-to-roll data were taken. For this portion of the overall investigation, the F/A-18E model was tested with the baseline wings that did not contain any of the instrumentation previously noted for the new wings. Details of the experimental procedures used for both the static and free-to-roll investigations can be found in reference 10.

WHAT STATIC TESTING IS NECESSARY?

Data Granularity

One important aspect of experimental wind tunnel testing has always been "how much data is necessary". One major conclusion of this program has been that it is necessary to take data in increments of angle of attack at least as small as 0.5° in the region where wing stall occurs. This requirement is illustrated in figure 3, where it may be noted that if the data had been taken either in 2° or 1° increments, the sharp break in the lift curve would not have been measured, and the potential for wing drop may have been missed.

Static Forces and Moments

One question that arose during the AWS Program was whether one could rely solely on figures of merit derived from static data taken during a transonic model test to provide the certainty needed that a new aircraft would or would not be susceptible to uncommanded lateral motions during its flight operations. Static figures of merit, or FOMs, are very important because they are intended to predict wing drop/rock behavior and, consequently, will enter into the decision of doing FTR testing or not. Comparing static test results with the FTR response data has provided a

rational basis for assessing the merits of using standard test techniques for the prediction of AWS events. A review of selected results from the investigations of four configurations will be made in order to define which static test measurement techniques should be employed to meet these requirements.

The sets of data for the four models were chosen as being representative of when both traditional (TFOMs) and alternate (AFOMs) figures of merit indicated that AWS activity would be presented and where these figures of merit indicated some activity, but none was present. Three of the TFOMs chosen for this analysis were lift coefficient C_L, rolling-moment coefficient C_ι and root mean square of rolling moment $C_{\iota,rms}$. In addition, three of the AFOM from reference 9 are also included.

One is now faced with the problem of defining which criteria are indicative of an AWS event. Figure 4 presents criteria that have been used traditionally to predict the onset of an AWS event. First, sharp breaks in lift-curve slope have traditionally been used as an indicator of an abrupt stall, which because of its nature may be asymmetric. Sudden or rapid variations in either rolling-moment coefficient or root mean square of rolling moment can signify rapid flow topology changes as angle of attack changes. The angle of attack at which these curves have a spike or peak is used as the criteria to indicate AWS activity for these two TFOMs and also for the AFOMs. However, as will be shown, where AWS activity is initiated is a matter of conjecture, and it could be argued that this activity starts at some angle of attack prior to that indicated by the peak. For those cases in which wing bending moments were measured, a change in the slope of these curves is used as the criteria.

Angles of attack at which AWS activity are indicated are then summarized in a "stoplight" chart. The stoplight chart also presents color-coded results measured during the pitch-pause phase of free-to-roll testing. During FTR pitch-pause tests, the model was released from a wings-level condition, and the resulting motions were recorded. A discussion of the color-coded rating system is given in the Free-To-Roll Figure of Merit section of this paper.

AV-8B. Four configurations of the AV-8B have been selected for discussion, and include those with the trailing-edge flap at 10°, 100% LERX at M = 0.5 and 0.75, and with the trailing edge flap at 25°, 100% LERX and 65% LERX at M = 0.50. The TFOMs and AFOMs are presented in figures 5 to 8 and compared to FTR results in figures 9 to 12. Note that symbols have not been used on any data figures for clarity. However, data was recorded in increments of angle of attack at least as small as 0.5°. Data shown on the stoplight charts are presented as a function of model pitch angle θ rather than angle of attack, since during FTR testing θ can be held constant whereas angle of attack α varies during the model rolling motions. When α or θ = 0°, these angles differ only by tunnel upflow angularity that averaged about +0.10°.

For the trailing edge flap at 10°, there is a marked difference in the magnitude of the lift-curve slope decrease between a Mach number of 0.50 and 0.75 (fig. 5). At M = 0.50, there is a slight drop in the lift curve slope at α = 7.5°, whereas there is a much sharper decrease in slope at α = 8.5° at M = 0.75 that could be indicative of AWS activity. However, as can be seen in figure 10, free-to-roll results showed no FTR lateral activity in this angle of attack range. The changes in wing bending moments noted at α = 8° on figure 10 are consistent with the decrease in lift curve slope. Also shown in figures 9 and 10 are the CFD predictions[8] of the break in the lift curve at M = 0.5 and 0.75. As can be seen, the predicted break in lift curve slope at M = 0.50 occurred about 3° higher than that measured. However, good agreement is noted between the CFD prediction and wind tunnel at M = 0.75.

Figure 5 also shows a difference in the character of rolling-moment coefficient between M = 0.5 and 0.75. At M = 0.5, no FTR lateral activity was noted, despite the sharp increase in rolling moment indicated in figure 5 at α = 16°. The very large asymmetries in rolling moment that were present at M = 0.75, are more typical of the behavior one might expect where uncommanded lateral motions might be present and, in fact, were experienced during the FTR tests (fig. 10).

At M = 0.5, there is a gradual increase in rolling-moment RMS, starting of about α = 12°. The increase in RMS is probably more an indication of buffet onset than any AWS activity. Buffet onset also occurs where there is a break in the axial force coefficient C_A curve. As seen in figure 5, the break in C_A also occurs at angle of attack of 12°. At M = 0.75, buffet onset occurs at α = 8°. Using the criteria previously described, AWS activity would be possible at α = 12° where the rolling moment RMS curve peaks for M = 0.75. Note that rolling-moment RMS returns to a lower level at an angle of attack greater than 14° after the wing has totally stalled. Based on the foregoing results, it should be obvious that trying to predict AWS activity depends on looking at more that a single balance component.

A summary of the free-to-roll characteristics for the AV-8B model for M = 0.5 with 25° flaps and the 100% LERX is presented in figure 11. For this configuration, some of the TFOMS and AFOMs predict AWS activity, but these predictions seem to occur randomly at various angles of attack.

However, for the AV-8B with the 65% LERX (fig. 12), several of the figures of merit predict AWS activity at θ = 14 to 14.5°, and severe AWS activity was experienced in the FTR tests. Note that there were also false predictions of activity near α = 10°. Wing rock occurred with flaps on schedule at θ = 14° to 14.5°.

For the AV-8B, both rolling moment and RMS rolling moment appear to be the significant figures of merit, and the results suggest that any future program include these measurements. The results of the static portion of the tests on the AV-8B also suggest a need to conduct FTR tests.

F/A-18C. The traditional and alternate figures of merit for the F/A-18C with δ_{le} = 6°, δ_{te} = 8° and δ_a = 0° (6°/8°/0°) at M = 0.80 to 0.90 are presented in figures 13 and 14 respectively. The first angle corresponds to leading-edge flap deflection, the second angle corresponds to the trailing-edge flap deflection, and the third angle corresponds to the aileron bias. These data are summarized in figure 15. At all Mach numbers, there are very significant breaks in the lift curves that are in marked contrast to those shown previously for the AV-8B. Figure 15 indicates that severe FTR lateral activity occurred at the angles of attack at which the lift curves break, even though there are lift-curve breaks at lower α's at which there is no activity. Note that FTR lateral activity always occurred at angles of attack at which the flaps are not on schedule. An examination of figure 15 suggests the difficulty of predicting AWS activity from the TFOMs and AFOMs. At all three Mach numbers, the figures of merit sometimes reliably predicted activity, and sometimes they falsely predicted activity. Also shown in figure 15, are the CFD predictions[8] of the break in the lift curve at M = 0.85 and 0.9. As can be seen, the predicted break in lift curve slope at M = 0.90 occurred about 1° lower than that measured.

For the F/A-18C configuration, lift-curve slope, rolling moment and RMS rolling moment appear to be significant FOMs, such that any future program should include these measurements.

Pre-production F/A-18E. The traditional and alternate figures of merit for the F/A-18E with flap settings of 6°/8°/4°, 10°/10°/5°, and 15°/10°/5° at M = 0.90 are presented in figures 16 and 17. Figure 18 presents some typical wing bending-moment data that were measured during an earlier entry in the 16FTT. These data are summarized in figures 19 to 21. The lift curves for the 6°/8°/4° and 10°/10°/5° flap settings have very significant breaks, similar to the F-18C. However, FTR lateral activity was already present, having started some 1° to 1.5° sooner than what would have been predicted by the breaks in lift curves (figs 19 and 20). For the 10°/10°/5° flap setting, all the figures of merit including the CFD FOM[7] line up and essentially predicted lateral activity. It is interesting to note that even though the time averaged C_l data indicates significant variation with α, the unsteady $C_{l,rms}$ data is smoother. Note that while FTR lateral activity is present with flaps on schedule, these results are for a model of the pre-production F/A-18E aircraft[1] and not are representative of the production aircraft[1]. For this configuration, lift-curve slope and rolling moment tended to predict AWS activity at angles of attack higher than where FTR lateral activity was present. However, in the absence of any FTR data, the results of the static portion of this investigation on the pre-production F/A-18E clearly show a need for FTR testing of this configuration.

F-16C. The traditional and alternate figures of merit for the F-16C with δ_{le} = 10° and δ_{te} = 0° at M = 0.80 and 0.90 are presented in figures 22 and 23 respectively. These data are summarized in figure 24. Except for some relatively small peaks noted for the $C_{l,rms}$, curves, this was a relatively benign configuration.

For the F-16C configuration, the TFOMs predicted that some AWS activity would be present, but no FTR lateral activity was present.

Wing Pressures

A series of tests were conducted early in the AWS program (ref. 1), on an 8-percent F/A-18E model with new set of wings that were heavily instrumented with static-pressure taps, and unsteady-pressure gauges. These wings were not used during the free-to-roll tests.

Steady Pressures. An example of the steady pressure distributions acquired on the F/A-18E model is given in figure 25. Distributions are presented at angles of attack both below wing stall and above wing stall for a flap setting of 10°/10°/5°, where the first angle corresponds to leading-edge flap deflection, the second angle corresponds to the trailing-edge flap deflection, and the third angle corresponds to the aileron bias. The pressure data are presented for various spanwise

wing stations, or butt lines, seen in the sketch in figure 25. The first pressure distribution, shown by the circles, was taken at an angle of attack of 8.0°, before the stall occurred in the mid-wing region. Abrupt stall occurred immediately thereafter as angle of attack increased by a small increment. The squares are for an angle of attack of 9.0°, which is after the stall for the wing panel at the mid-wing span locations. As seen during the stall process, significant regions of low pressures--that is, coefficients toward the top of the vertical axis--collapse as the separation process moves forward up and over the mid-wing region. Evidence of the stall process is apparent in Rows A, E, G, and I, but is clearest in Row G and is consistent with legacy oil flow images. Further details of this investigation are discussed by McMillin[3]. This type of information is invaluable in determining the flow physics associated with AWS events, and the critical spanwise stations where the separation is most severe.

Unsteady Pressures An analysis of the unsteady pressure measurements has been made by Schuster[5]. Figure 26 shows pressure coefficient time history data acquired at a single pressure transducer on the E-row near the center of the wing box at Mach 0.9. The location of this transducer is circled on the image of the planform at the bottom of the figure. Time histories are plotted in one-degree angle of attack increments from 6.5° to 9.5°. The pressure coefficient plotted in this figure is the complete pressure coefficient, as opposed to just the fluctuating component of the pressure.

This figure clearly shows the progression of the shock wave forward on the wing as the angle of attack is increased into the AWS region. At 6.5°, the pressures measured by the transducer are very stable and constant across the time slice. At 7.5°, the first hint of a shock moving onto this chordwise location is seen in the discrete spikes in the pressure time history. By 8.5°, the spikes are much more prevalent, and finally at 9.5° the time history is saturated with pressure spikes as the shock moves back and forth across the pressure transducer. Hwang and Pi[19] observed a similar unsteady pressure character in their buffet and wing rock analysis of a model of the F-5A aircraft during transonic wind-tunnel tests.

Further research[5] is required into how unsteady pressures might be readily used to screen for AWS. Generally, a normal test program cannot afford to include unsteady pressure transducers nor the time to record and analyze the data. However, a definite recommendation is that if unsteady pressure transducers are required, they should be included on both wings of the aircraft as opposed to just the single wing in this study. Lateral phenomena could be readily extracted and separated from longitudinal phenomena using time synchronized pressure data from both wings. This would likely provide an entirely new insight into the AWS phenomenon. In addition, the overall coverage of unsteady transducers should be increased over that used in the present study. This would probably require a larger scale model and it would surely require a more complex and capable dynamic data acquisition system than used in this analysis.

Pressure Sensitive Paint

In addition to obtaining steady and unsteady pressure measurements, pressure sensitive paint (PSP) imaging was used to gather global information on the pressures influencing the wing drop. This technique, which offers the advantage of continuous pressure information across the wing (in contrast to the discrete pressure taps seen in figure 25), was highly successful in this transonic application. As seen in figure 27, the pressure pattern correlates well with comparable Veridian 8-ft Transonic Tunnel oil flows, despite the fact that the Veridian test used a different model wing than that tested at Langley. The correlation of PSP images with force and moment data is reported in more detail by McMillin[5]. As discussed in reference 3, trade offs are required in operational test time using the technique, since considerable setup time is required between runs for model cool-down, image calibrations, etc.

CORRELATION OF STATIC AND FREE-TO-ROLL BALANCE MEASUREMENTS

One of the FTR major requirements[10] in the design of the free-to-roll rig was that the force balance was to be retained and used during testing. Even though there were risks involved with this requirement, having the force balance proved to be invaluable, in particular from a safety standpoint in being able to monitor model loads during FTR testing. Another concern was that the forces and moments measured by the balance during free-to-roll testing would be erroneous. However, this turned out not to be the case. A comparison of the measured forces and moments between FTR and static testing is presented in figures 28 to 31. Data for the static tests were pitch-pause, whereas the FTR tests were conducted using the pitch sweep mode. These results are for the largest model tested, the AV-8B, with the 100% and 65% LERX and with 10°

and 25° trailing edge flap deflection. Excellent agreement is shown for the two test modes for the longitudinal data for those cases when no free-to-roll activity is present. However, when free-to-roll activity is present, large variations in some aerodynamic coefficients do occur due to large changes in bank angle.

FREE-TO-ROLL TO FLIGHT CORRELATIONS

Free-To-Roll Figure of Merit

In order to discern the level of lateral activity from free-to-roll tests, figures of merit were also developed. This figure of merit needs to resolve "significant" activity from the inconsequential. Taking into account amplitude alone could lead to the wrong conclusions since the motion may have a large amplitude change but the motion is so slow that it would be easily controlled. Taking into account just the magnitude of rates or accelerations alone could also lead to the wrong conclusions since a large acceleration with a small amplitude oscillation might not be controllable but would not lead to a large deviation in the aircraft trajectory. Or, the acceleration might be favorable if it is returning the aircraft to a wings level condition.

Initially, amplitude measured during the pitch-pause phase of free-to-roll testing, was used as a figure of merit. During FTR pitch-pause tests, the model was released from a wings-level condition, and the resulting motions were rated based on an arbitrary color-coded rating system. This system was based on the ensuing amplitude of bank angle, where green represented an amplitude of less than 10°, yellow an amplitude between 10° and 20° and red any amplitude greater than 20°. Initial ratings for a selected configuration of each of the four models tested are presented in figure 32. Note the large number of "yellow" and "red' events that occur for the F/A-18C and F/A-18E at low angles of attack. These events can generally be characterized as being slow-period large-amplitude motions.

Therefore, a new figure of merit[11] was developed that accounted for both amplitude and rate. The FOM $(p_{P\text{-}V})_{max}$ is defined as the absolute value of the amplitude change from a peak to its nearest valley divided by the time it takes to roll through this amplitude. This method captures wing drops that have no overshoots and wing rock that has sinusoidal motion. A color-coded system was also devised for this FOM where green represented values of $(p_{P\text{-}V})_{max}$ less than 50, yellow had values between 50 and 100 and red any value greater than 100. While still somewhat arbitrary, the various levels were established after a review of the results from the four models showed data falling predominately within these three bands.

The current ratings for the same four configurations shown previously in figure 32 are presented in figure 33. Although the same range is used for all the models, there is no expectation that the level of lateral activity means the same for all airplanes given their different sizes and inertias. As can be seen, the previous the low α "red" severe events for the F/A-18E have now become "green" not significant events. Also note that the "green" event occurring at α = 15.5° (fig. 32) for the AV-8B has become a "red" event.

Roll Rate Correlation

A correlation of roll rate to roll acceleration has been performed for each of the four configurations tested during the FTR tests and these results are presented in figure 34. All data collected during the pitch-pause phase of the FTR tests are given for each configuration. Note that all configurations have been plotted to the same scales. The highest roll rates measured were for the F-18C at angles of attack in which the flaps were off schedule. There appears to be no effect of Mach number, except for the AV-8B at M = 0.3. (Note the data with the circle symbols.)

Roll rates for the F/A-18E determined in the wind tunnel and flight[12] are shown in figure 35. A direct comparison of these data cannot be made because the wind tunnel model was not dynamically scaled to the aircraft, and the aircraft stability augmentation system was not represented in the FTR test technique. However, the trends of roll rate variation with acceleration are very similar.

Angle of Attack Correlation

A comparison of FTR activity to flight data for the pre-production F/A-18E is shown in figure 36 for Mach numbers of 0.8 and 0.9. The data shown is where both the airplane and model had approximately the same flap settings and Mach number at the time of a lateral activity event. As can be seen, there is good agreement between the wind tunnel and flight. However, this correlation only shows unacceptable lateral activity, not the type of lateral activity. Note that while FTR lateral activity is present with flaps on schedule, these results are for a model of the pre-production F/A-18E aircraft[1] and are not representative of the production aircraft[1].

Figures 37 and 38 shows a comparison of angles of attack for wing rock/drop between flight and wind tunnel for the AV-8B with the 100% LERX and the 65% LERX. Flight data for the 100% LERX is only available for Mach numbers greater than 0.5, whereas flight data exists for the 65% LERX at Mach numbers from about 0.22 to 0.90. The ranges of wind-tunnel data presented are for "yellow or red" conditions. As can be seen, there is excellent agreement between the flight and wind tunnel data. The most noticeable difference between 100% and 65% LERX occurs at $M = 0.5$ where, unfortunately, there is no flight or wind tunnel data for 100% LERX. It should be noted, that any wing drop/rock activity noted is not considered an AV-8B aircraft operational problem.

Roll Damping Correlation

A correlation of roll damping between flight[20] and those measured in the wind tunnel are presented in figure 39. Roll damping is extracted from the roll angle time histories of the resulting motions when the model is released from some initial roll angle. Good agreement is noted in figure 39.

RECOMMENDATIONS

Based on extensive studies of static experimental figures of merit in the AWS Program for four different aircraft configurations, no one specific static FOM consistently flagged a warning of potential lateral activity only when actual activity was seen in the FTR experiments and, conversely, never flagged when FTR activity did not occur. However, these studies pointed out the importance of measuring and recording the RMS signals of the force balance. As reported by Lamar[23], however, many variables can serve as "relatively" dependable static FOMS when taken as a group. Included in this group should be measurements of wing bending for correlations to the corresponding CFD FOMs involving half-plane rolling moment[15].

If the experimental static FOMs indicate a potential lateral activity, it is recommended to proceed to FTR testing. It is essential that the FTR test program include at least three test approaches; continuous sweep, pitch pause, and roll offsets. Some further refinement of free-to-roll test procedures are expected as further analysis of the results reaches completion.

REFERENCES

1. Hall, R. M.; and Woodson, S: *Introduction to the Abrupt Wing Stall (AWS) Program.* AIAA-2003-0589, January 2003.
2. Chambers, J. R.; and Hall, R. M.: *Historical Review of Uncommanded Lateral-Directional Motions at Transonic Speeds.* AIAA-2003-0590. January 2003.
3. McMillin, S. N; Hall, R. M.; and Lamar, J. E.: *Understanding Abrupt Wing Stall with Experimental Methods.* AIAA-2003-0591, January 2003.
4. Woodson, S.; Green, B; Chung, J.; Grove, D.; Parikh, P.; and Forsythe, J.: *Understanding Abrupt Wing Stall (AWS) with CFD.* AIAA-2003-0592, January 2003.
5. Schuster, D.; and Byrd, J.: *Transonic Unsteady Aerodynamics of the F/A-18E at Conditions Promoting Abrupt Wing Stall.* AIAA-2003-0593, January 2003.
6. Forsythe, J.; and Woodson, S.: *Unsteady CFD Calculations of Abrupt Wing Stall Using Detached- Eddy Simulation.* AIAA-2003-0594, January 2003.
7. Parikh, P; and Chung, J.: *A Computational Study of the AWS Characteristics for Various Fighter Jets: Part I, F/A-18E & F-16C.* AIAA-2003-0746, January 2003.
8. Chung, J.; and Parikh, P.: *A Computational Study of the Abrupt Wing Stall (AWS) Characteristics for Various Fighter Jets: Part II, AV-8B and F/A-18C.* AIAA-2003-0747, January 2003.
9. Lamar, J. E.; Capone, F. J.; and Hall, R. M.: *AWS Figure of Merit (FOM) Developed Parameters from Static, Transonic Model Tests.* AIAA-2003-0745, January 2003.
10. Capone, F. J; Owens, D. B.; and Hall, R. M: *Development of a Free- To- Roll Transonic Test Capability.* AIAA-2003-0749. January 2003.
11. Owens, B; Capone, F. J.; Hall, R. M.; Brandon, J; and Cunningham, K: *Free-To-Roll Analysis of Abrupt Wing Stall on Military Aircraft at Transonic Speeds.* AIAA-2003-0750, January 2003.
12. Roesch, M; and Randall, B.: *Flight Test Assessment Of Lateral Activity.* AIAA-2003-0748, January 2003.
13. Green, B; and Ott, J.: *F/A-18C to E Wing Morphing Study for the Abrupt Wing Stall Program.* AIAA-2003-0925, January, 2003.
14. Kokolios; A., and Cook, S.: *Use of Piloted Simulation for Evaluation of Abrupt Wing Stall Characteristics.* AIAA-2003-0924, January 2003.

15. Woodson, S.; Green, B.; Chung, J; Grove, D.; Parikh, P; and Forsythe, J.: *Recommendations for CFD Procedures for Predicting Abrupt Wing Stall (AWS).* AIAA-2003-0923, January, 2003.
16. Cook, S.; Chambers, J.; Kokolios, A.; Niewoehner, R.; Owens, B.; and Roesch, M.: *An Integrated Approach to Assessment of Abrupt Wing Stall for Advanced Aircraft.* AIAA-2003-0926, January 2003.
17. Hall, R. M.; Woodson, S.; and Chambers, J. R.: *Accomplishments of the AWS Program and Future Requirements.* AIAA-2003-0927, January, 2003.
18. Bore, Cliff L.: *Post-Stall Aerodynamics of the Harrier GR1.* AGARD-CP-102 Fluid Dynamics of Aircraft Stalling. 1972.
19. Hwang, C.; and Pi, W.S.: "*Investigation of Steady and Fluctuating Pressures Associated With the Transonic Buffeting and Wing Rock of a One-Seventh Scale Model of the F-5A Aircraft.*" NASA Contractor Report 3061, November 1978. NOTE: Subsequently summarized, reduced, and published as: "*Some Observations on the Mechanism of Aircraft Wing Rock." AIAA Paper 78-1456, AIAA Aircraft Systems and Technology Conference*. Los Angeles, CA. August 21-23, 1978.
20. Stevenson, Scott W.; Holl, David; and Roman, Alan: *Parameter identification of AV-8B Wingborne Aerodynamics for Flight Simulator Model Updates*. AIAA-92-4506-CP, August 1992.

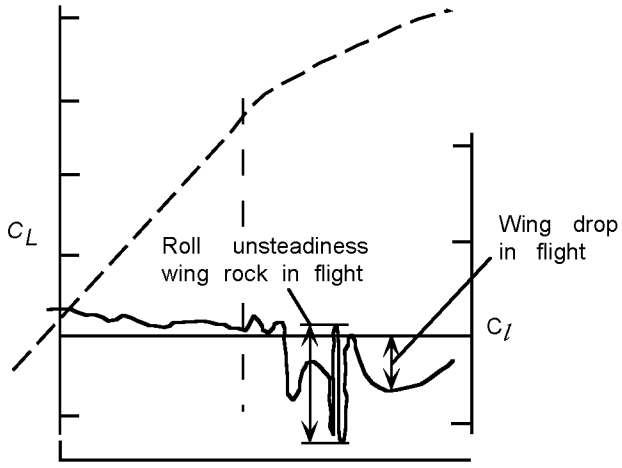

Figure 1. Roll unsteadiness of the Harrier from experimental wind tunnel data (ref. 18).

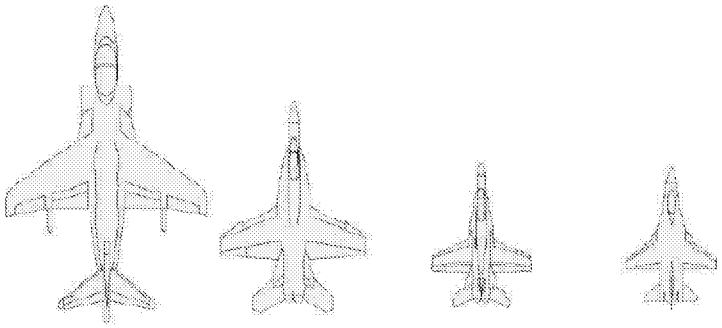

	AV- 8B	F/A-18E	F/A-18C	F-16C
Length, in.	81.27	54.99	39.18	37.25
Wing Area, ft^2	5.18	3.2	1.44	1.33
Span, ft	4.55	3.34	2.25	2.07
Weight, lbs	490	185	55	56
Inertia, s-ft^2	4	1.2	0.2	0.2
Scale, %	15	8	6	6.67
Static Forces & Moments	Yes	Yes	Yes	Yes
Force & Moment, rms	Yes	Yes	Yes	Yes
Unsteady Forces & Moments	No	Yes	No	No
Wing Bending Moments	Yes	Yes	No	Yes
Wing Bending Moments, rms	Yes	Yes	No	Yes
Free-To-Roll	Yes	Yes	Yes	Yes
Wing Pressures	No	Yes	No	No
Unsteady Wing Pressures	No	Yes	No	No
Pressure Sensitive Paint	No	Yes	No	No

Figure 2. Scope of Abrupt Wing Stall experimental investigations.

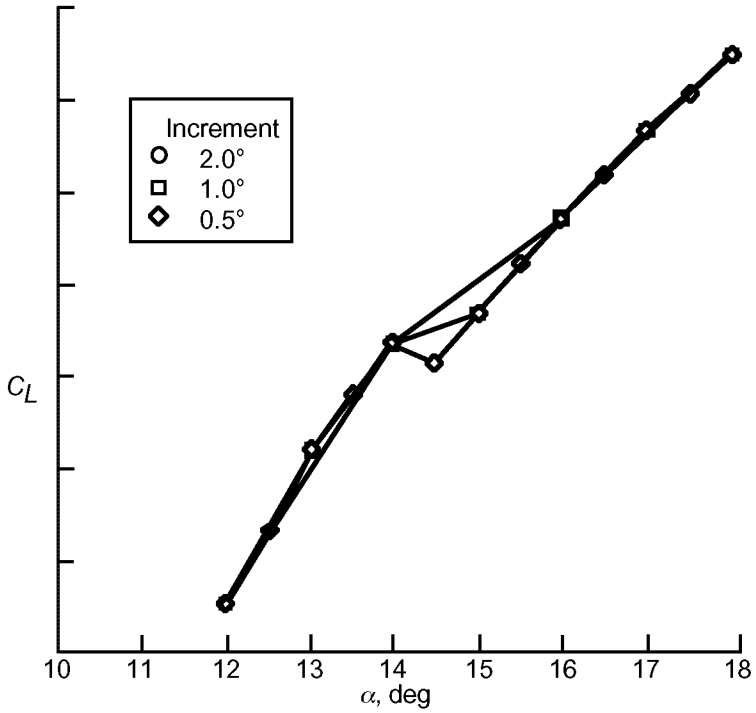

Figure 3. Effect of increment in angle of attack on test data.

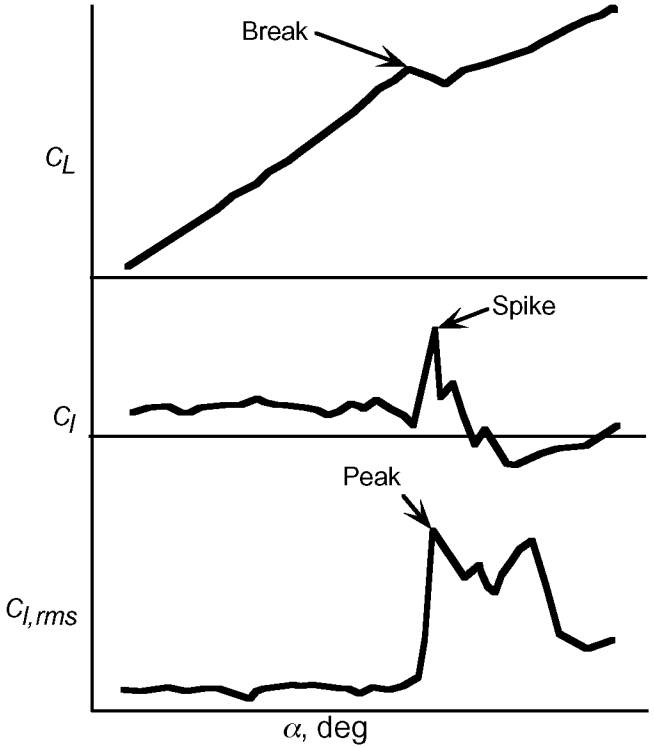

Figure 4. Definition of traditional figures of merit.

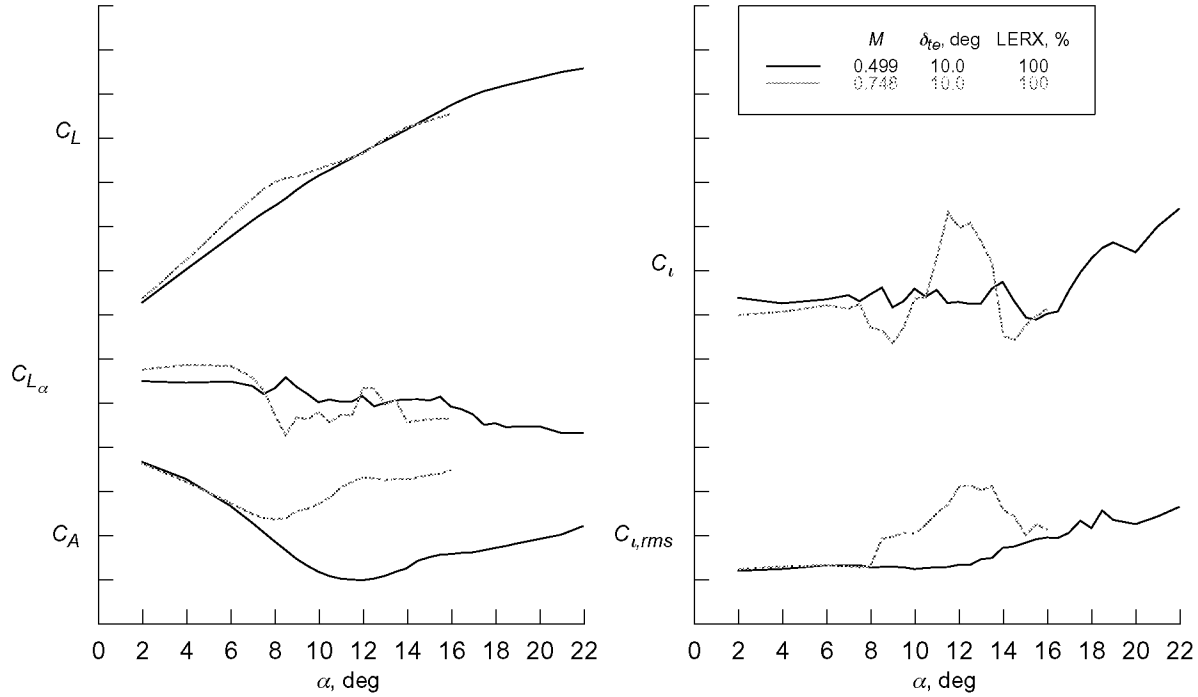

Figure 5. Traditional figures of merit for the AV-8B.

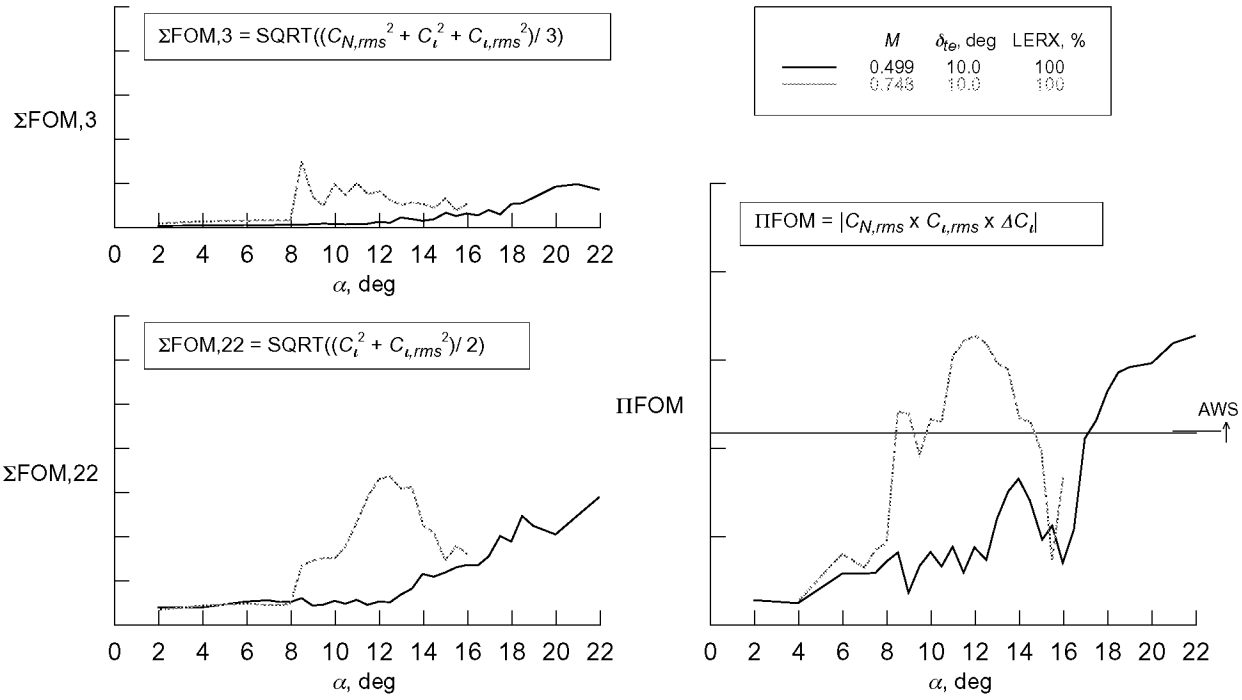

Figure 6. Alternate figures of merit for the AV-8B.

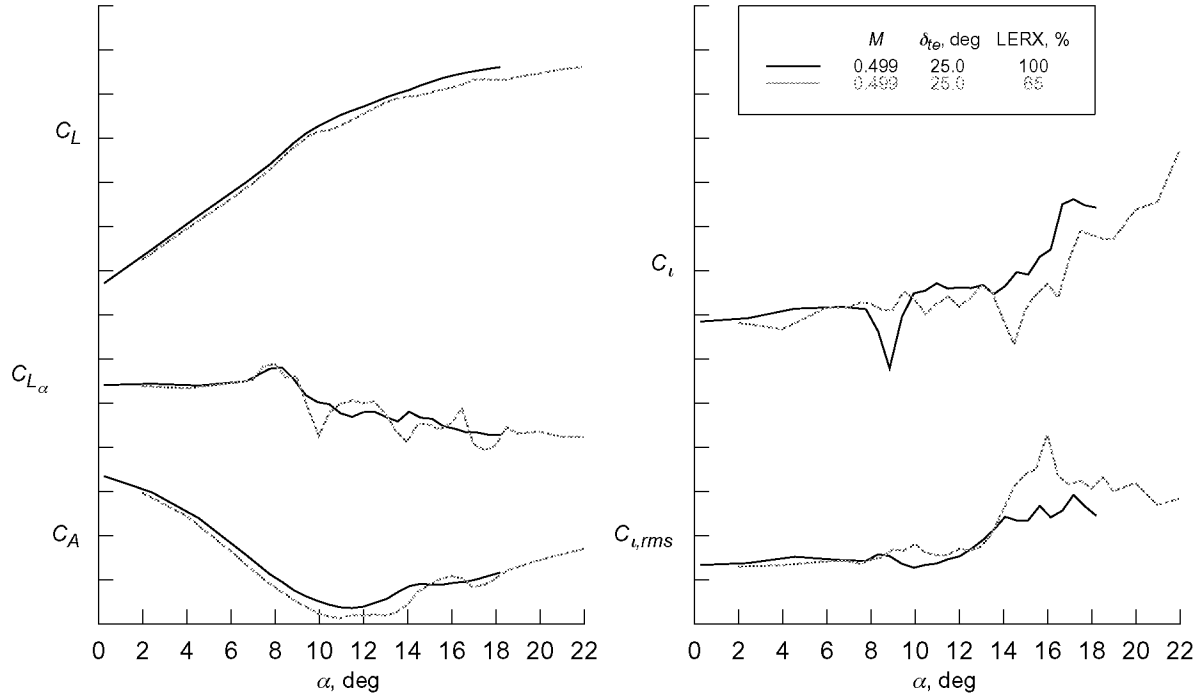

Figure 7. Traditional figures of merit for the AV-8B.

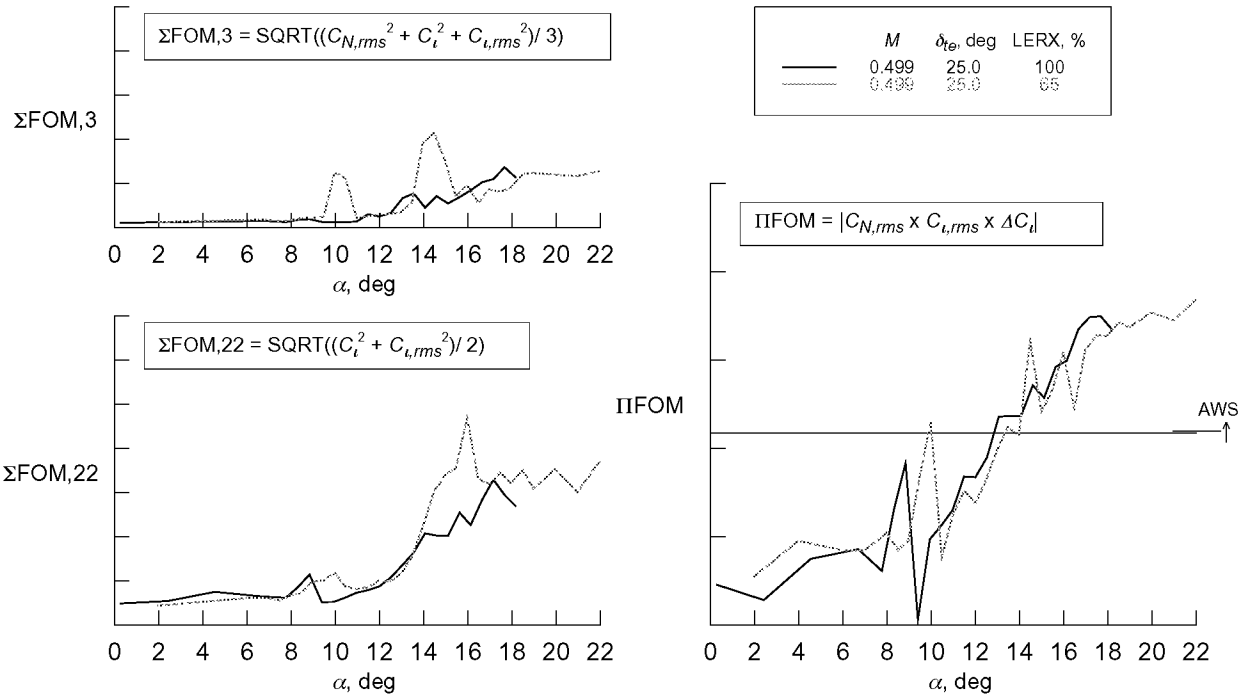

Figure 8. Alternate figures of merit for the AV-8B.

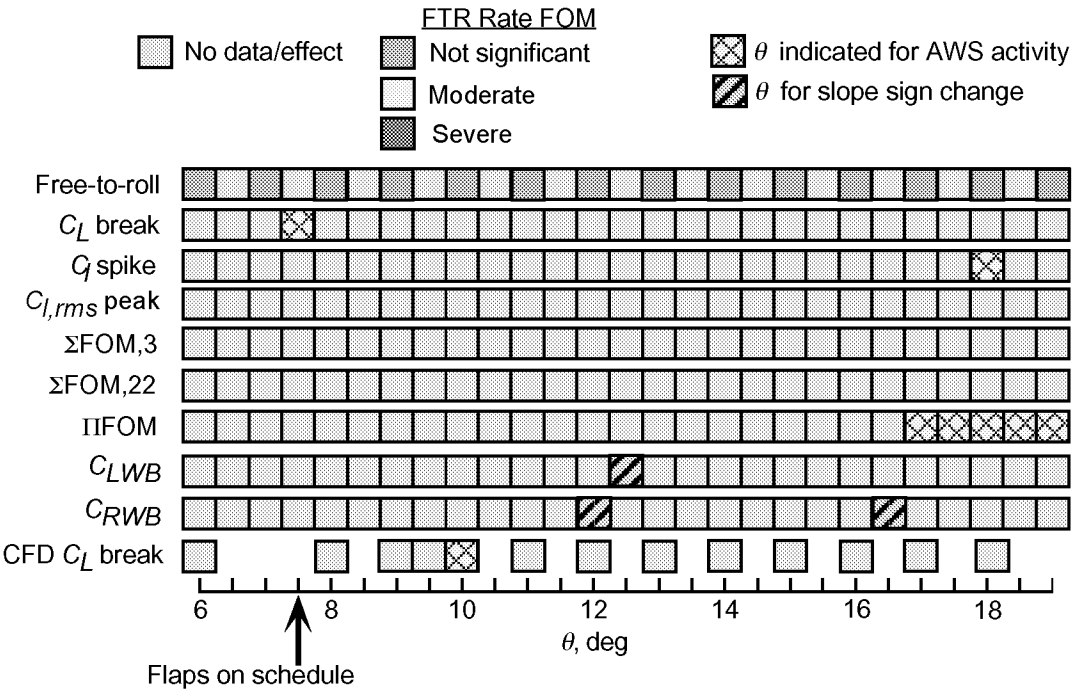

Figure 9. Stoplight chart for AV-8B with 100% LERX, $\delta_f = 10°$, $M = 0.50$.

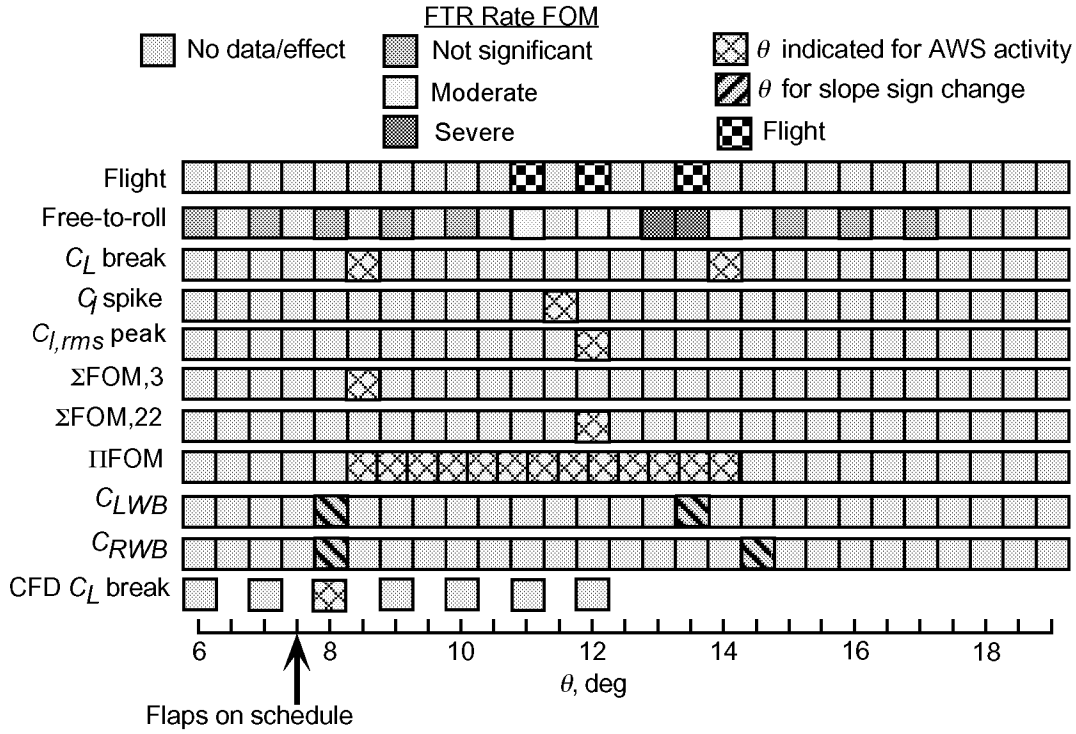

Figure 10. Stoplight chart for AV-8B with 100% LERX, $\delta_f = 10°$, $M = 0.75$.

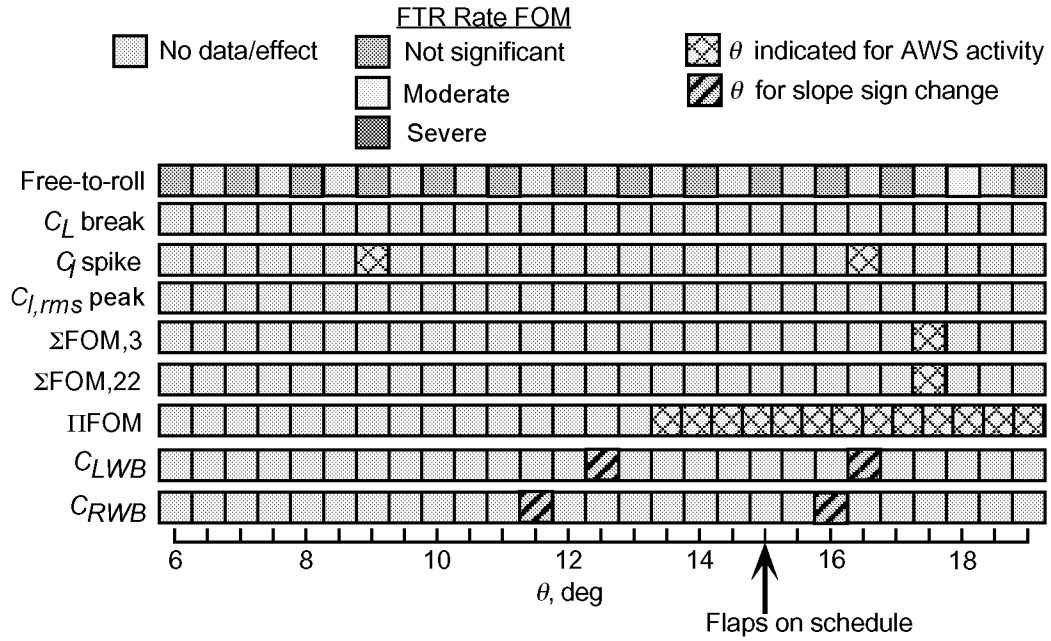

Figure 11. Stoplight chart for AV-8B with100% LERX, $\delta_f = 25°$, $M = 0.50$.

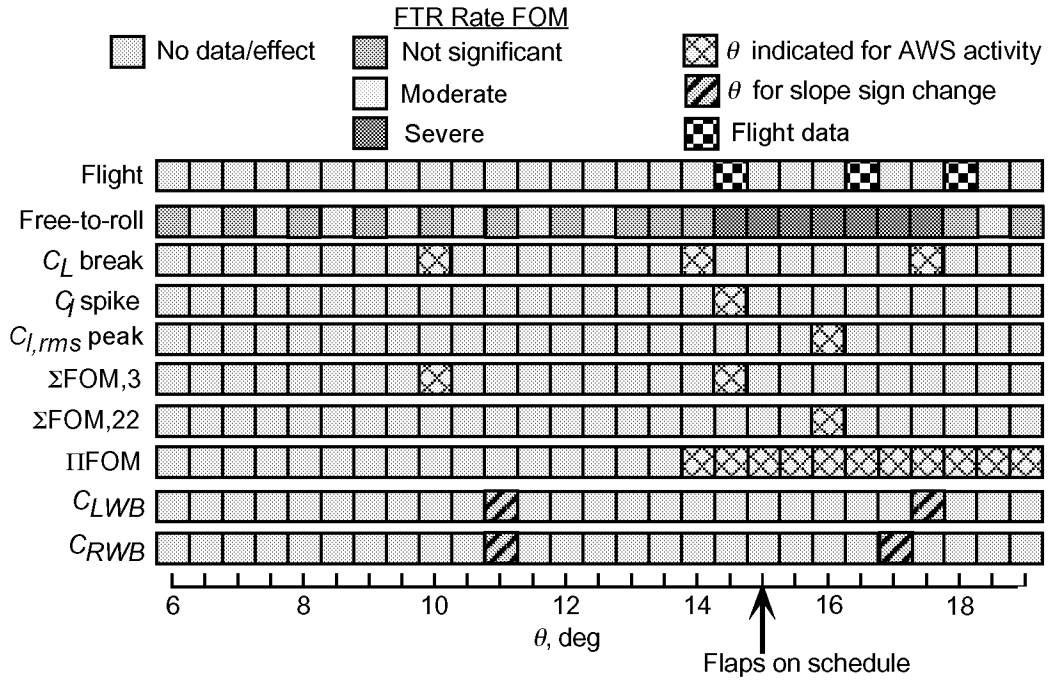

Figure 12. Stoplight chart for AV-8B with 65% LERX, $\delta_f = 25°$, $M = 0.50$.

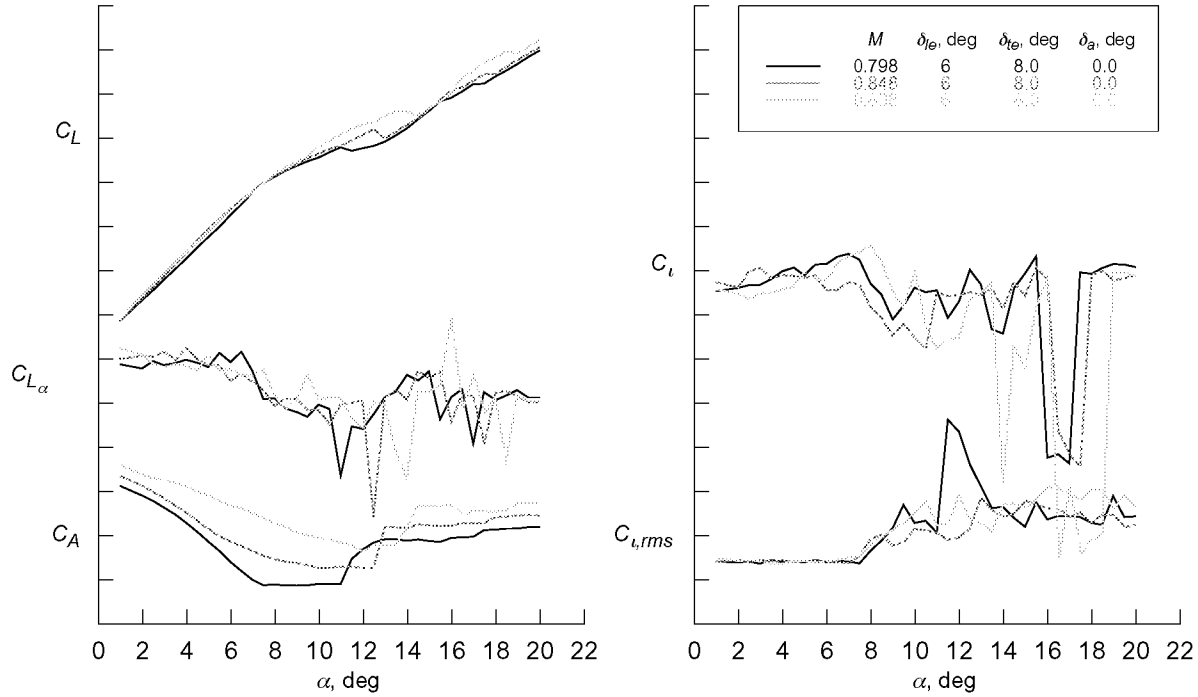

Figure 13. Traditional figures of merit for the F/A-18C.

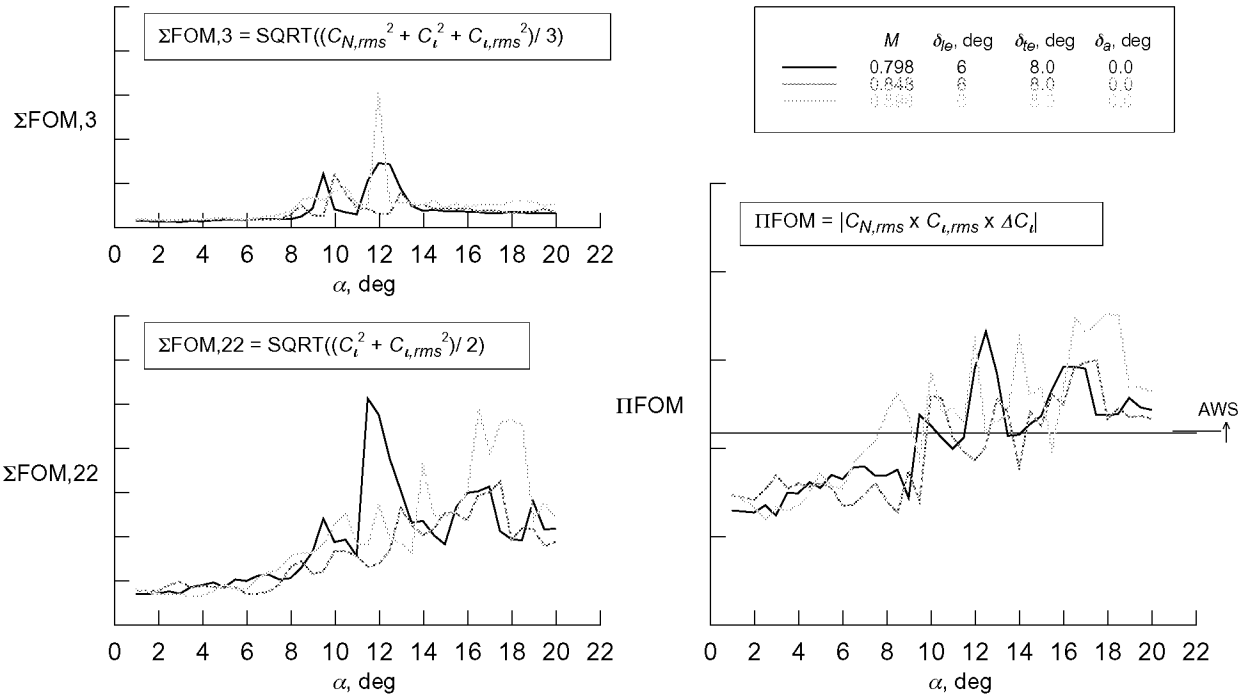

Figure 14. Alternate figures of merit for the F/A-18C.

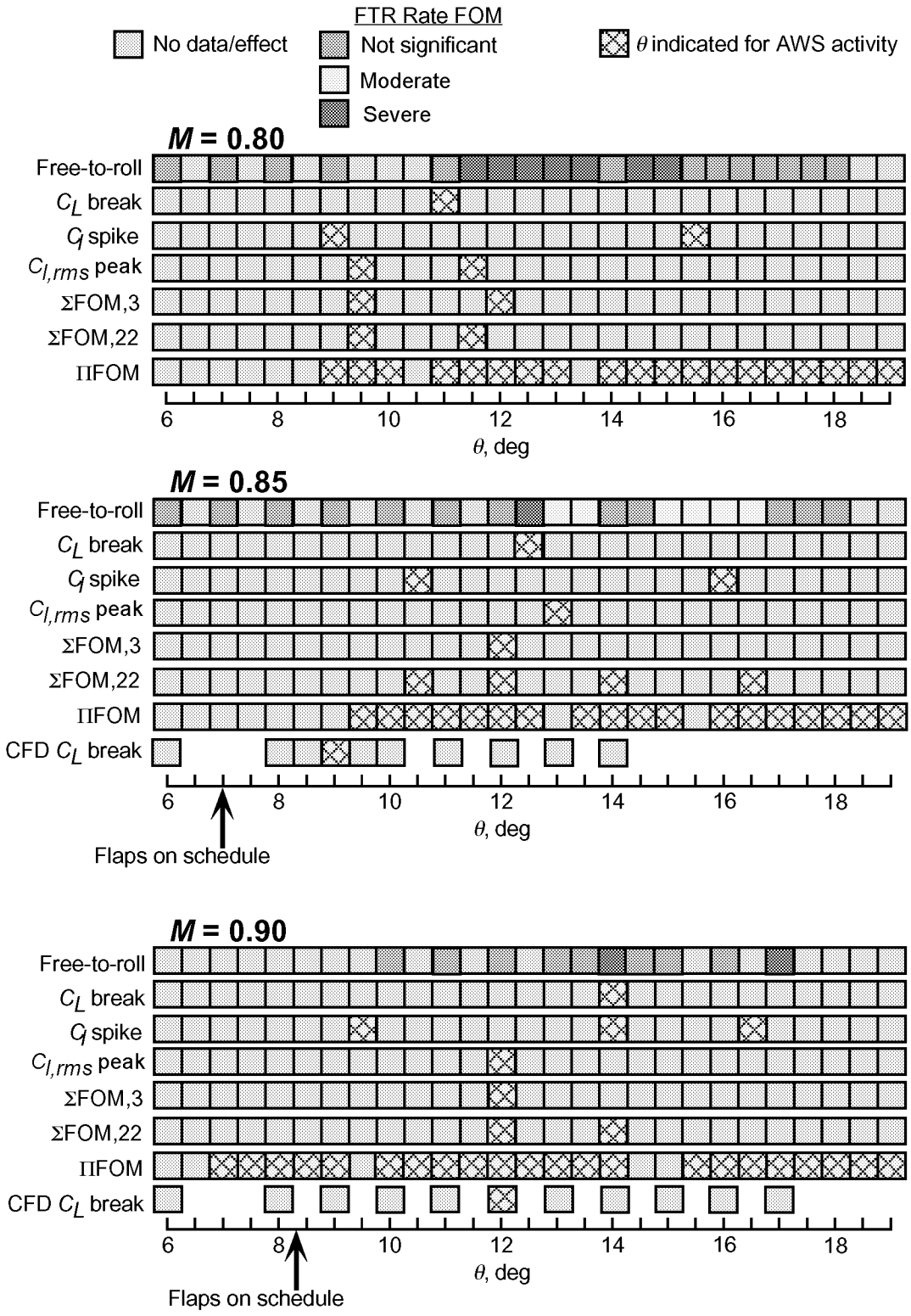

Figure 15. Stoplight chart for F/A-18C, $\delta_{le} = 6°$, $\delta_{te} = 8°$, $\delta_a = 0°$.

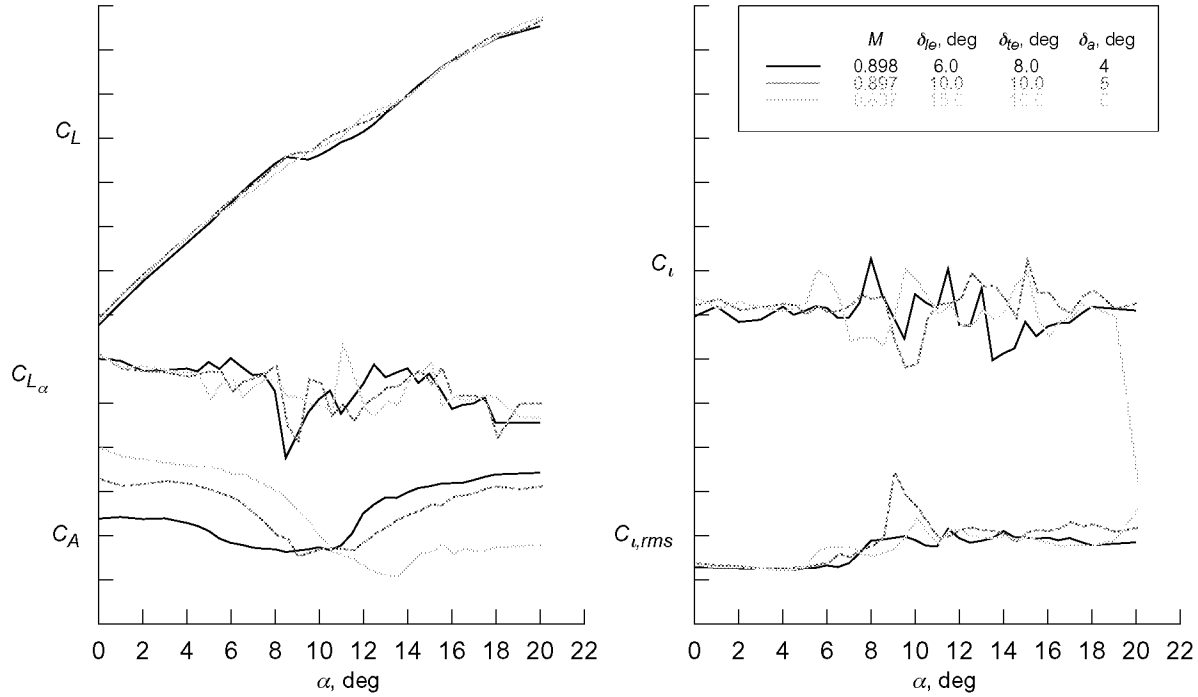

Figure 16. Traditional figures of merit for the pre-production F/A-18E.

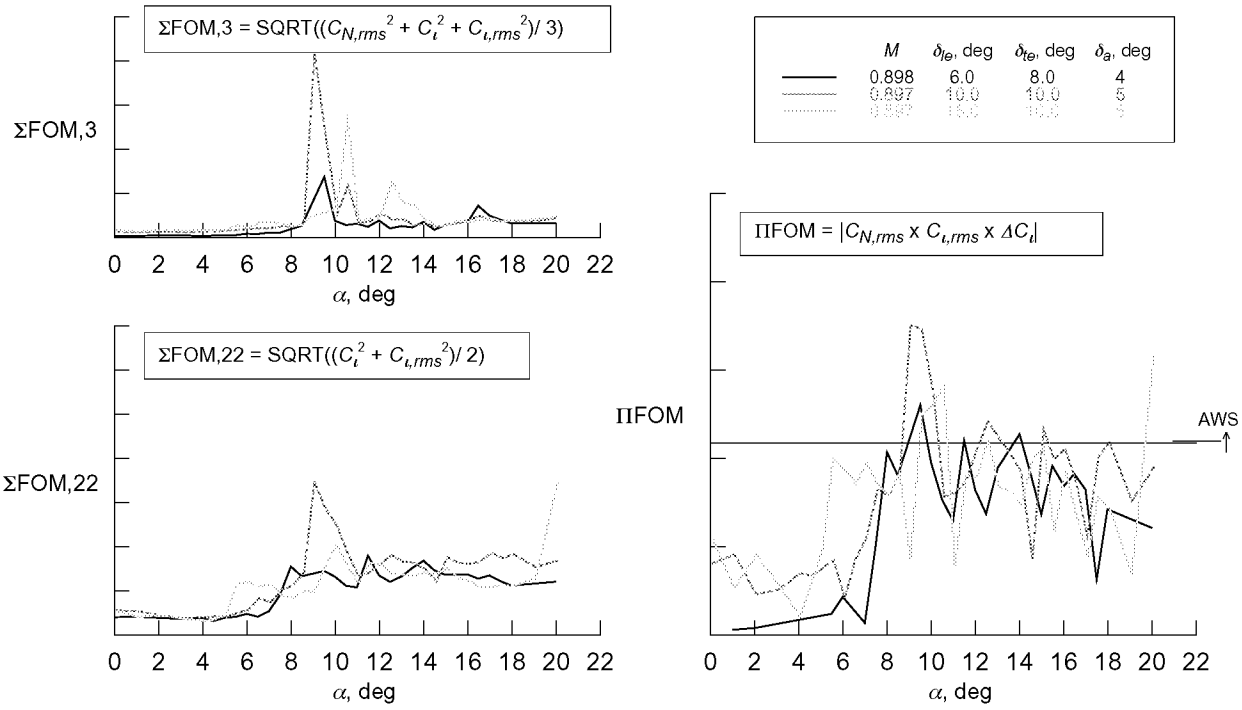

Figure 17. Alternate figures of merit for the pre-production F/A-18E.

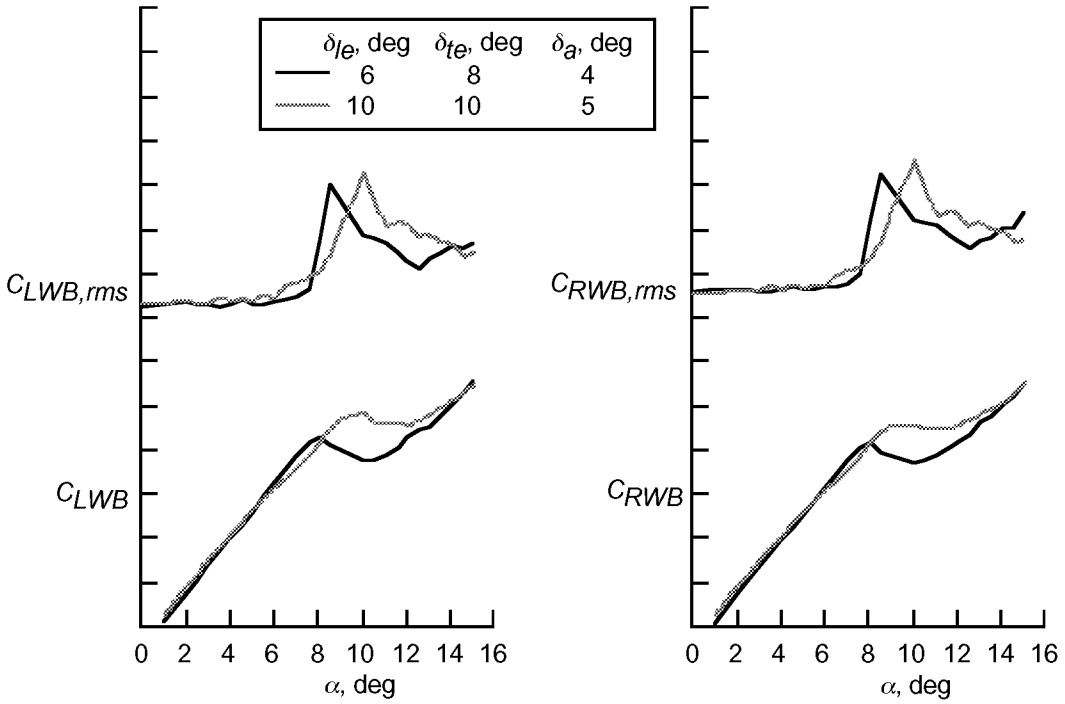

Figure 18. Wing bending moment characteristics for the pre-production F/A-18E, M = 0.90.

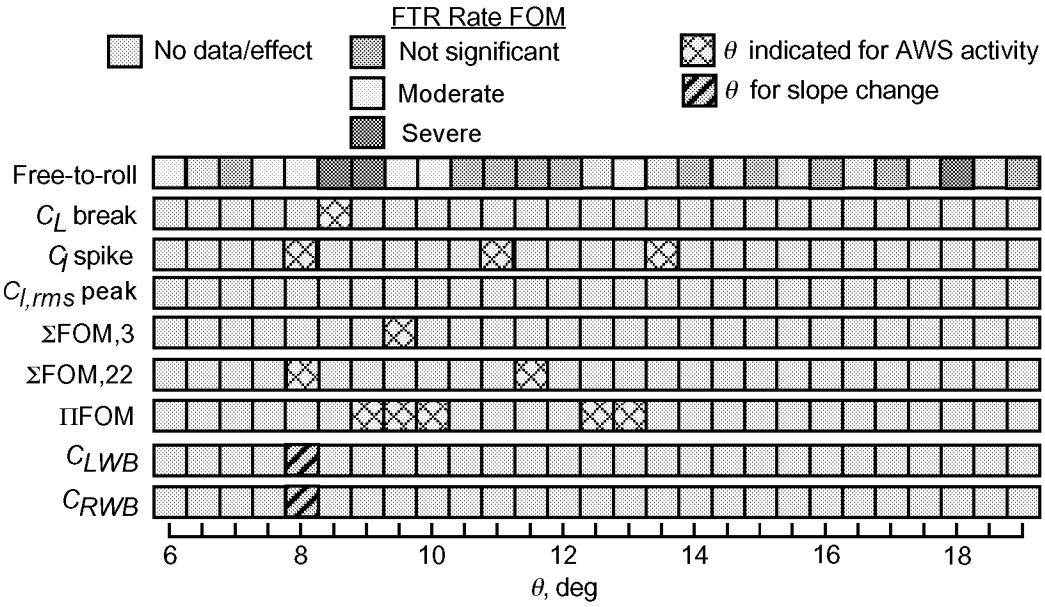

Figure 19. Stoplight chart for pre-productiion F/A-18E,
δ_{le} = 6°, δ_{te} = 8°, δ_a = 4°, M = 0.90.

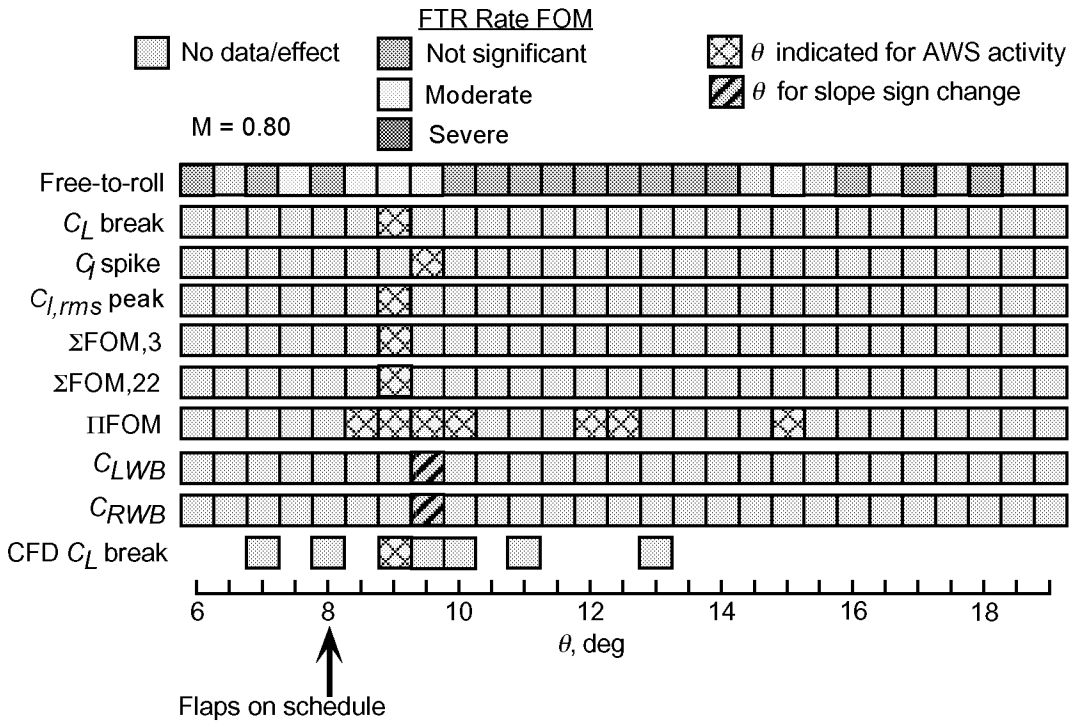

Figure 20. Stoplight chart for pre-production F/A-18E, δ_{le} = 10°, δ_{te} = 10°, δ_a= 5°, M = 0.90.

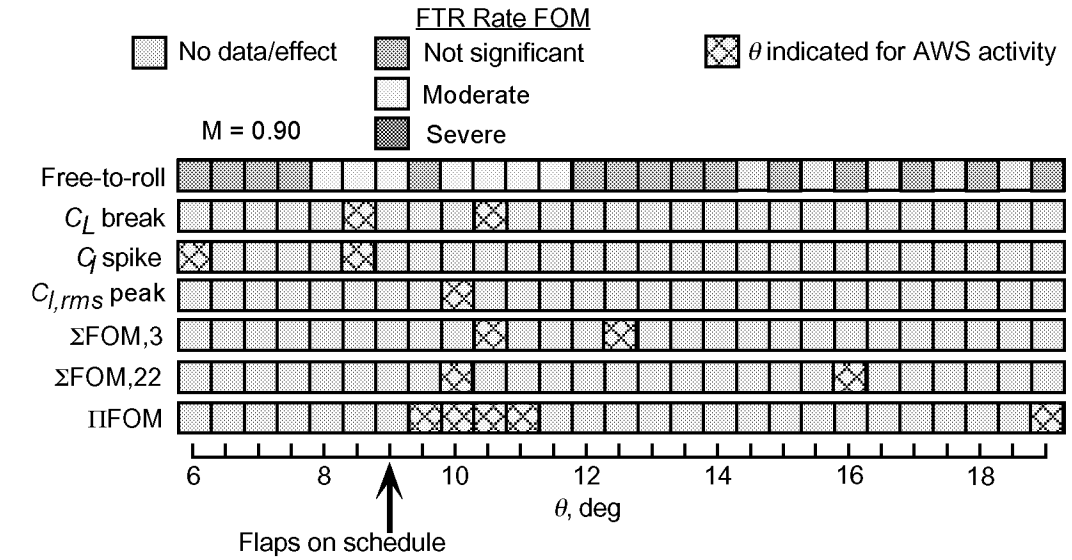

Figure 21. Stoplight chart for pre-production F/A-18E, δ_{le} = 15°, δ_{te} = 10°, δ_a = 5°, M = 0.90.

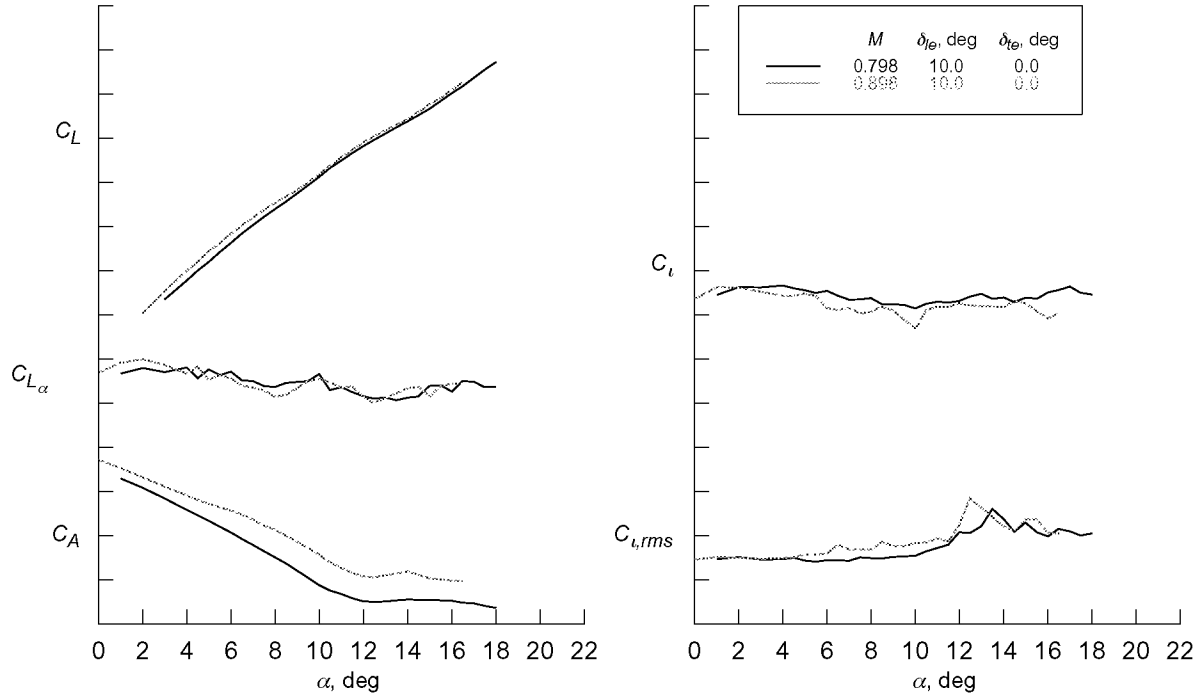

Figure 22. Traditional figures of merit for the F-16C.

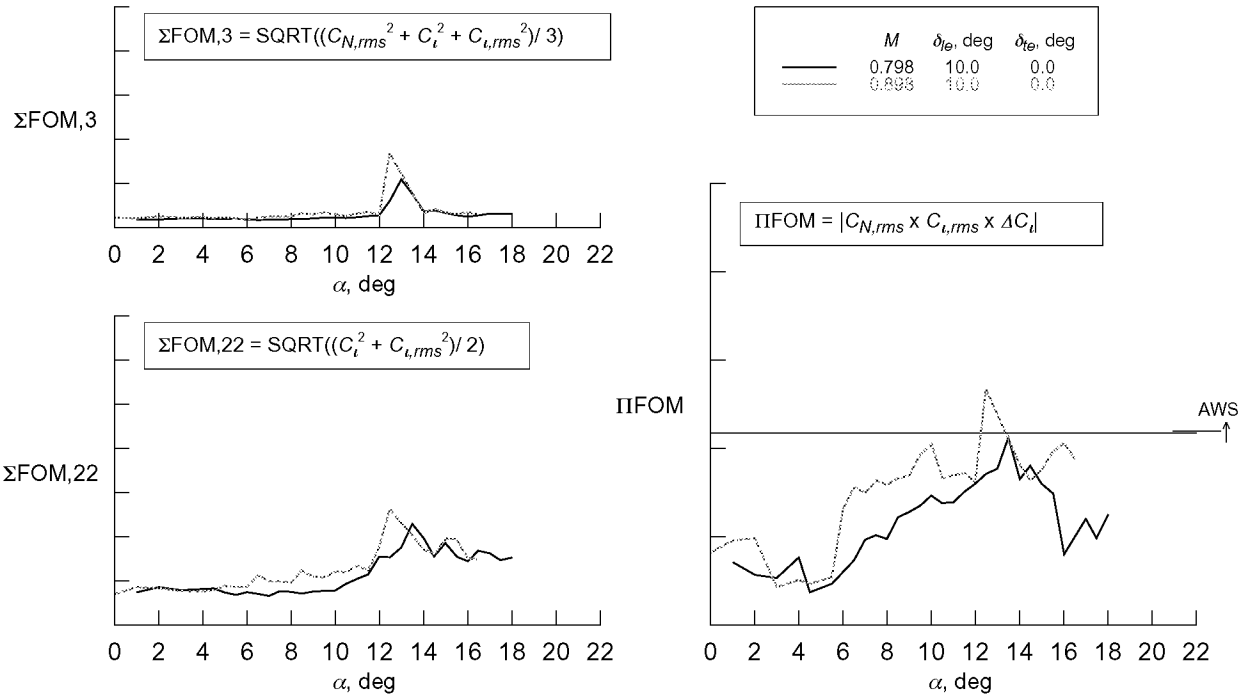

Figure 23. Alternate figures of merit for the F-16C.

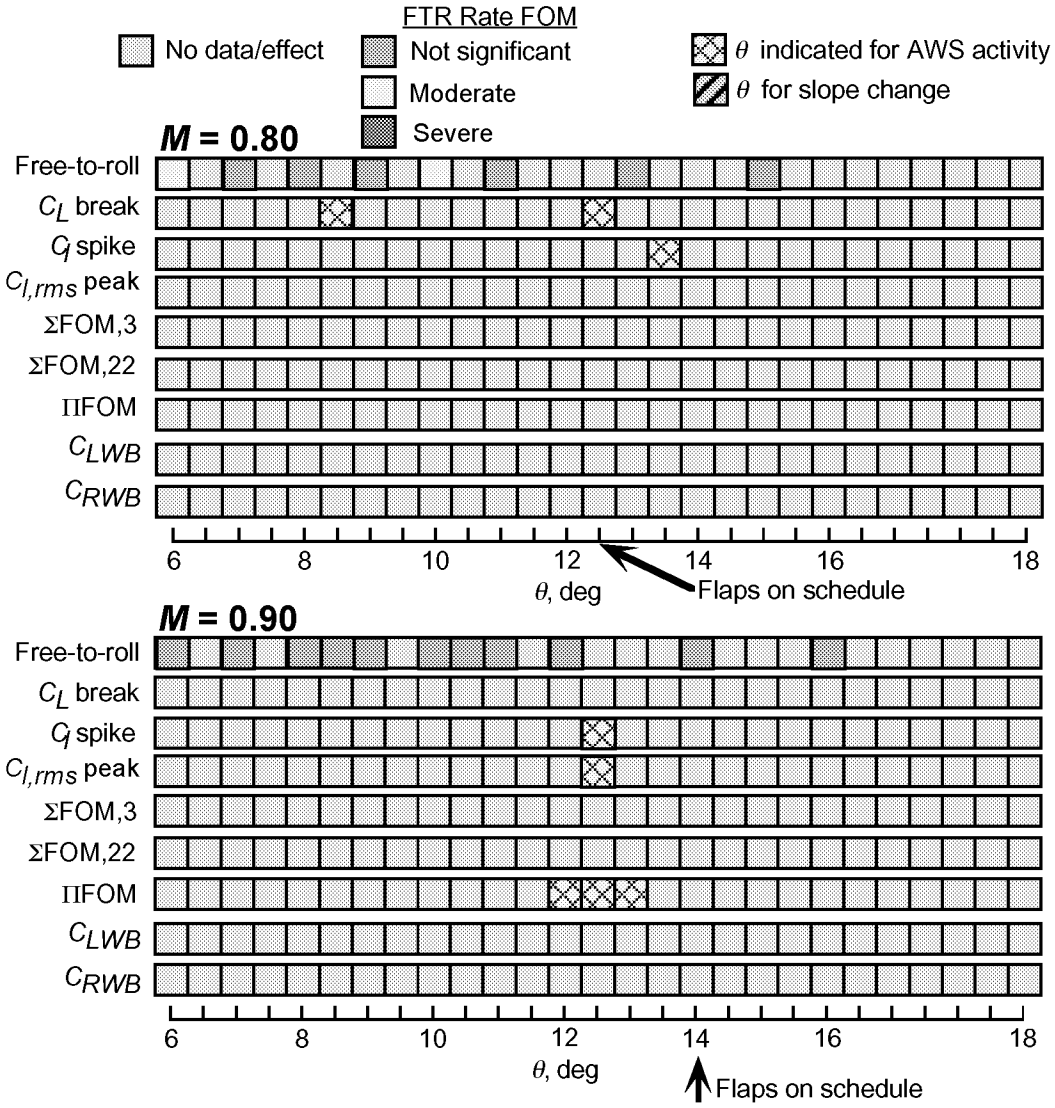

Figure 24. Stoplight chart for F-16C, δ_{le} = 10°, δ_{te} = 0°.

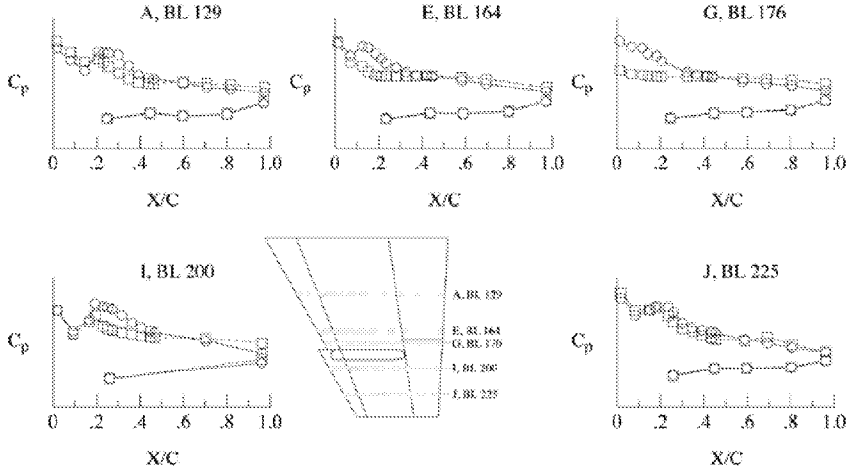

Figure 25. Steady pressures for F/A-18E, δ_{le} = 10°, δ_{te} = 10°, δ_a = 5°, M = 0.80. Cirdes, α = 8°, squares, α = 9°

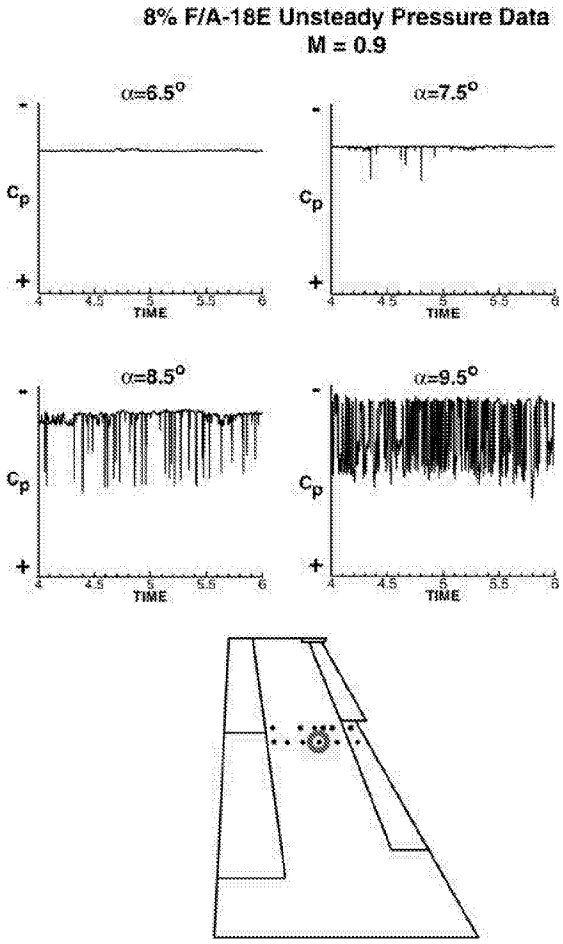

Figure 26. Pressure coefficient time history at a single point on the wing for a series of angles of attack, M = 0.90.

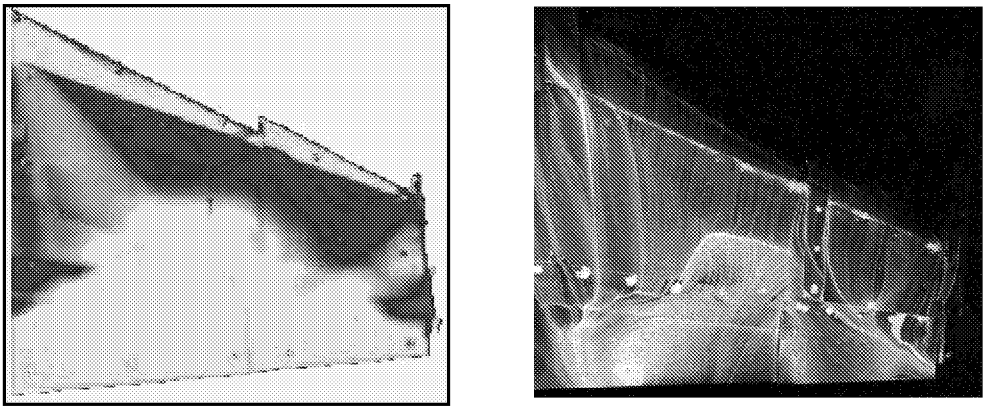

Figure 27. Comparison of PSP image to oil flow photograph.

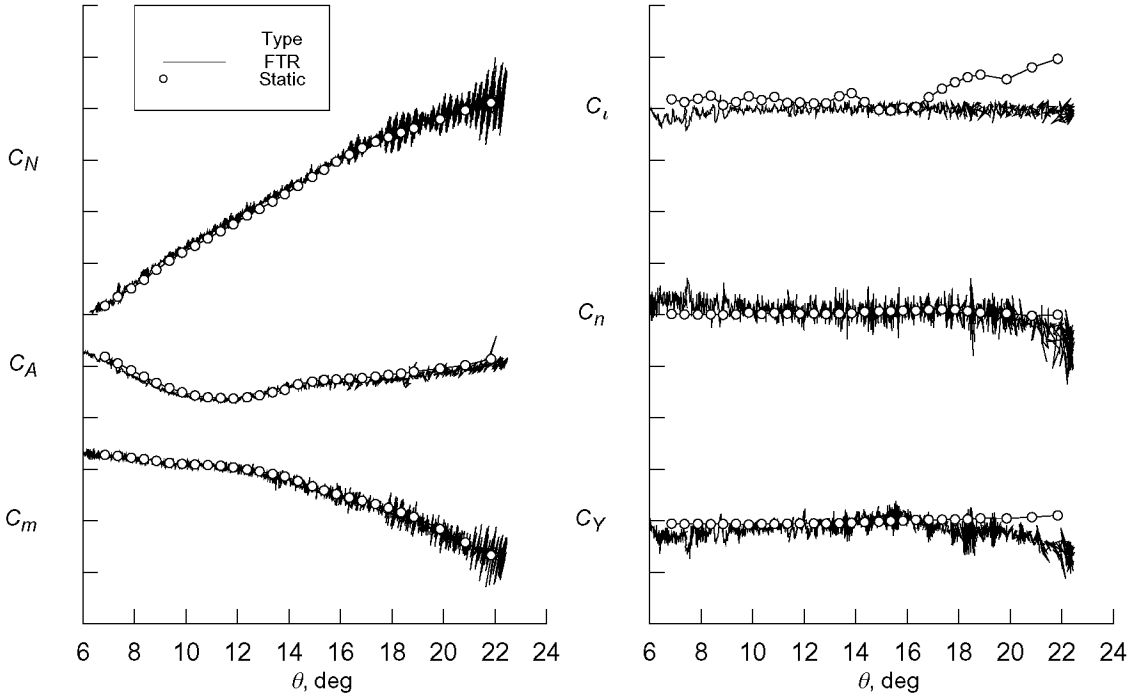

Figure 28. Comparison of static and free-to-roll aerodynamic characteristics for the AV-8B. 100% LERX, δ_{te} = 10.0°, M = 0.50.

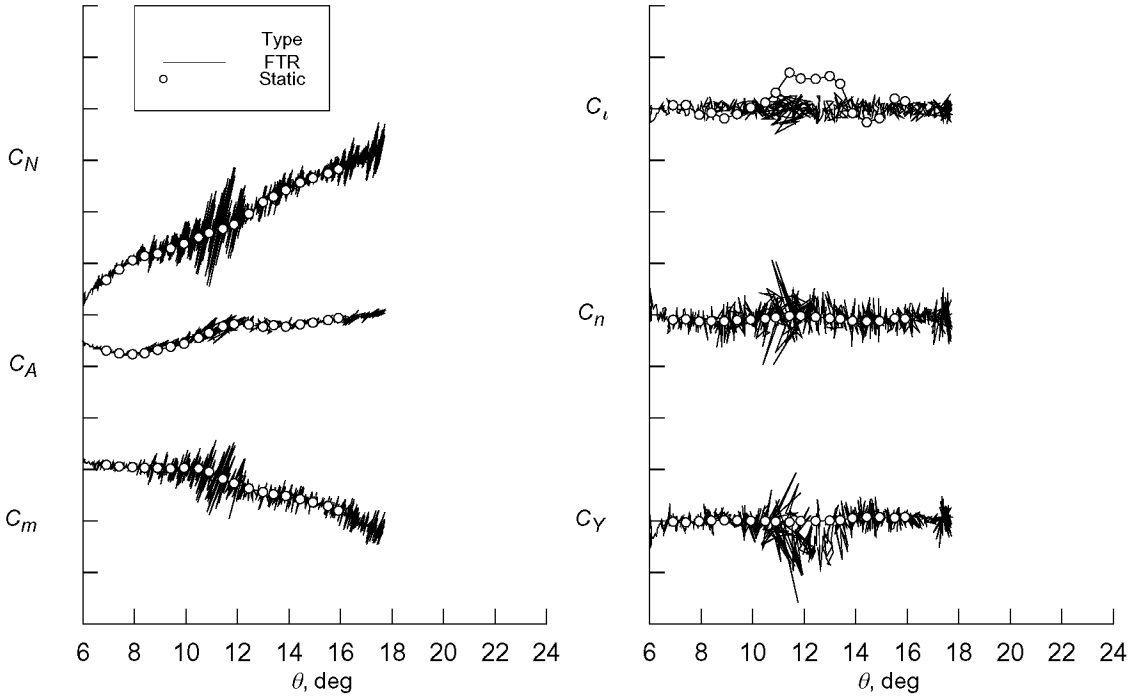

Figure 29. Comparison of static and free-to-roll aerodynamic characteristics for the AV-8B. 100% LERX, δ_{te} = 10.0°, M = 0.75.

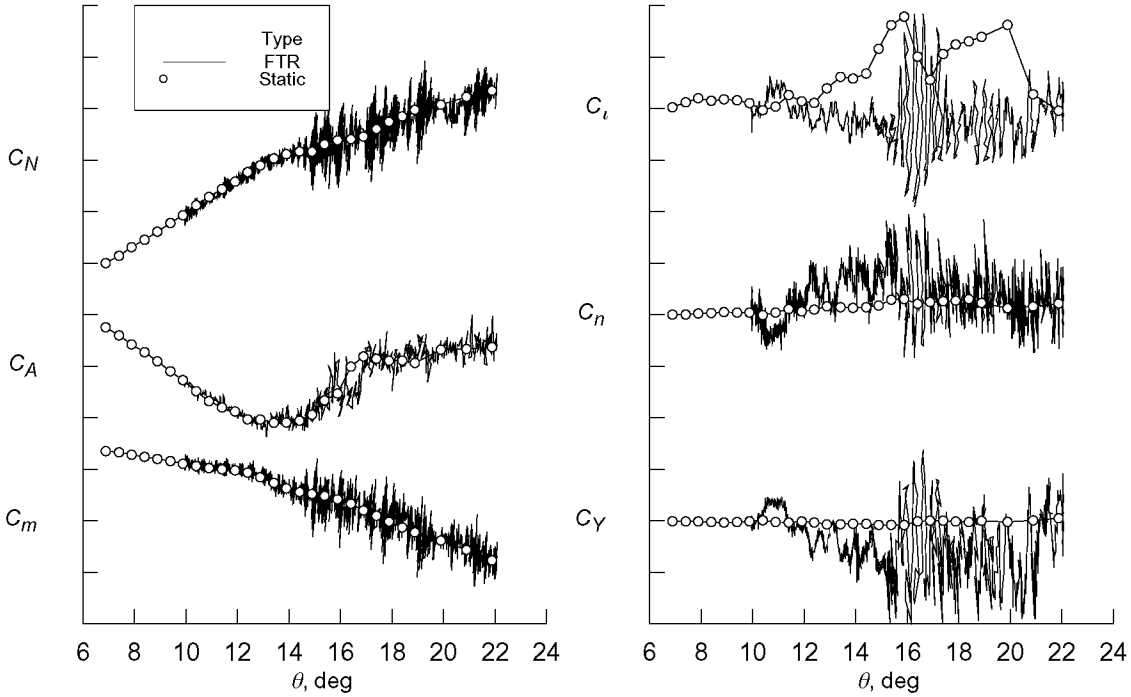

Figure 30. Comparison of static and free-to-roll aerodynamic characteristics for the AV-8B. 65% LERX, δ_{te} = 25.0°, M = 0.30.

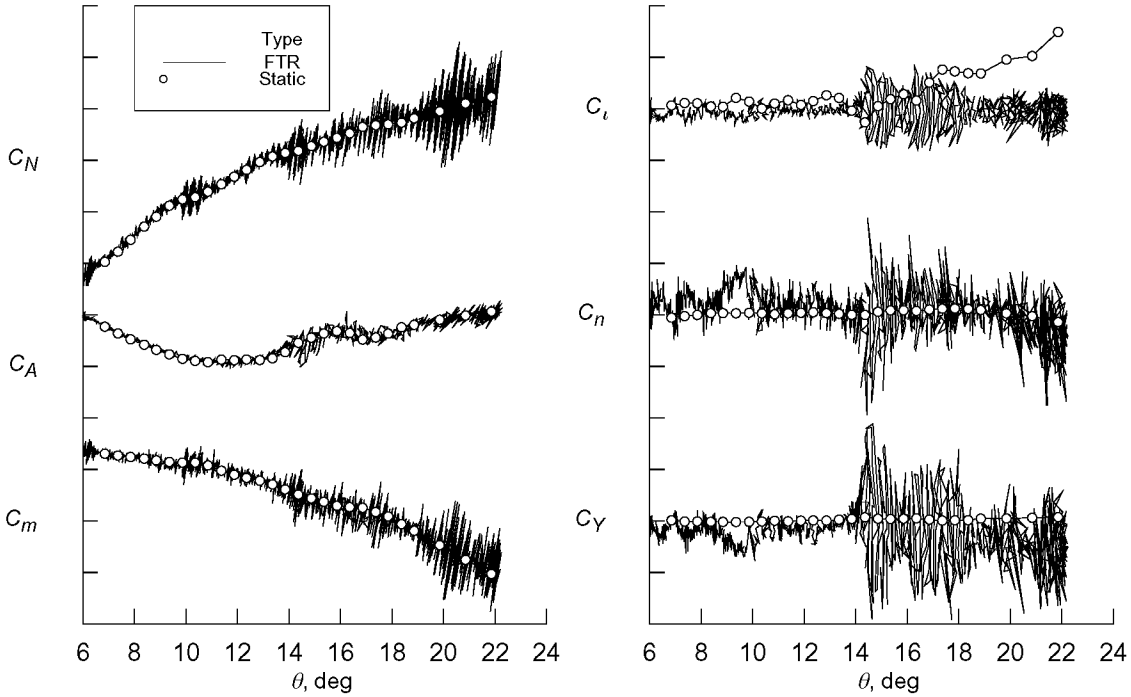

Figure 31. Comparison of static and free-to-roll aerodynamic characteristics for the AV-8B. 65% LERX, δ_{te} = 10.0°, M = 0.50.

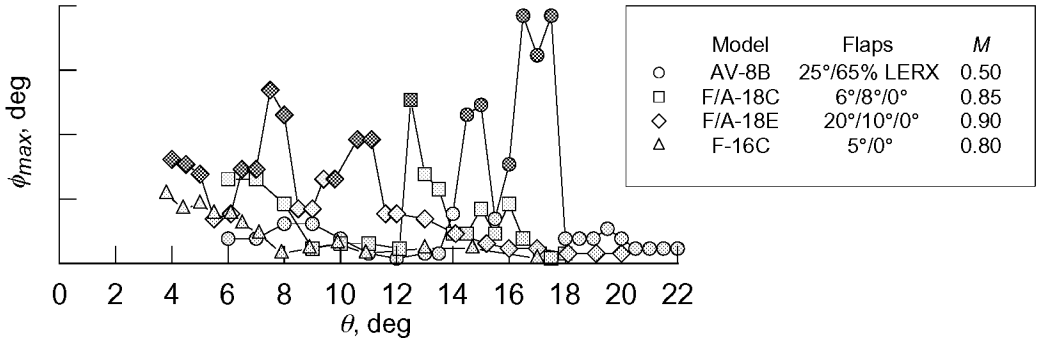

Figure 32. Initial ratings for a selected configuration of the models tested.

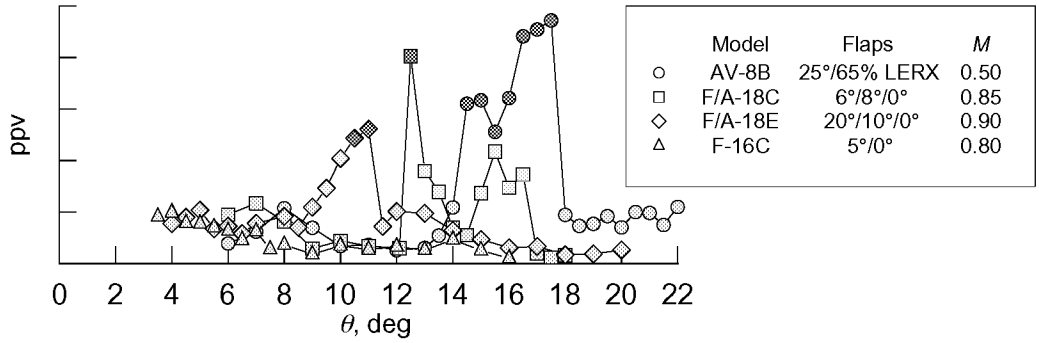

Figure 33. Current ratings for a selected configuration of the models tested.

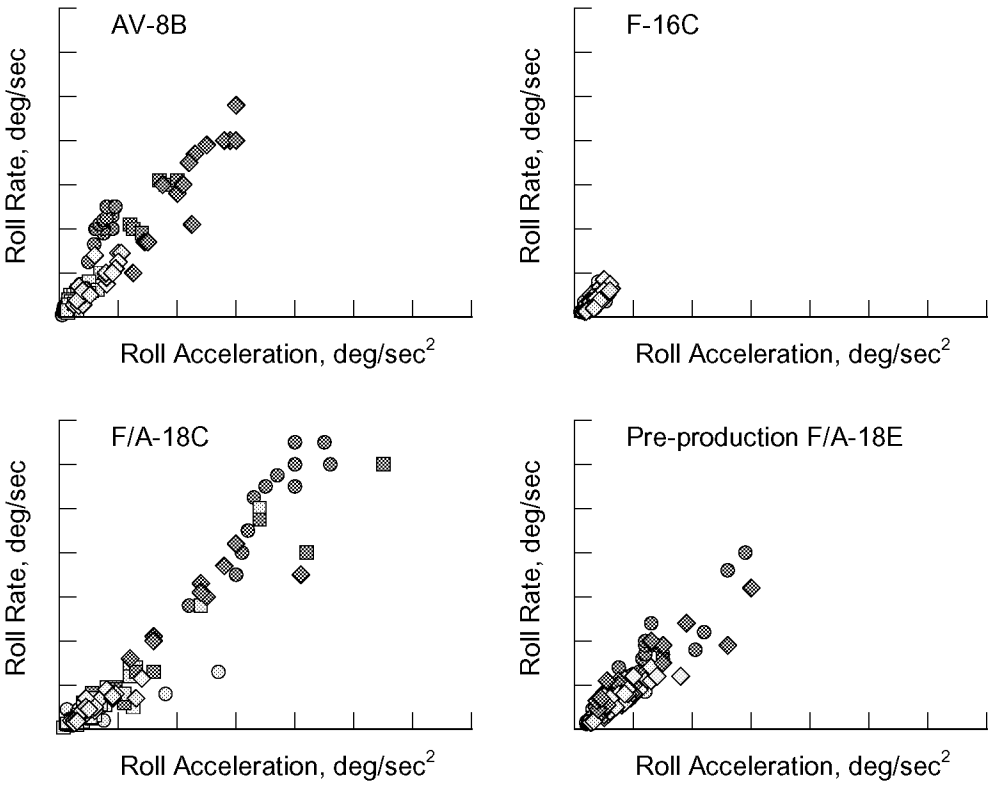

Figure 34. Roll rate characterisitcs for the four configurations tested.

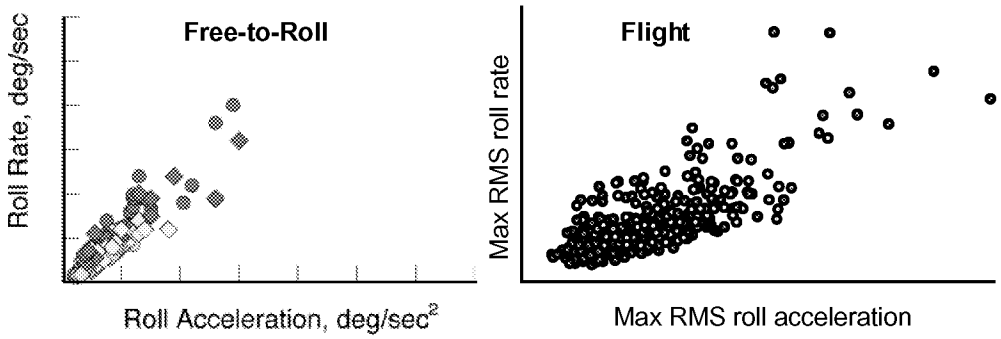

Figure 35. Comparison of free-to-roll and flight roll rate
for the pre-production F/A-18E.

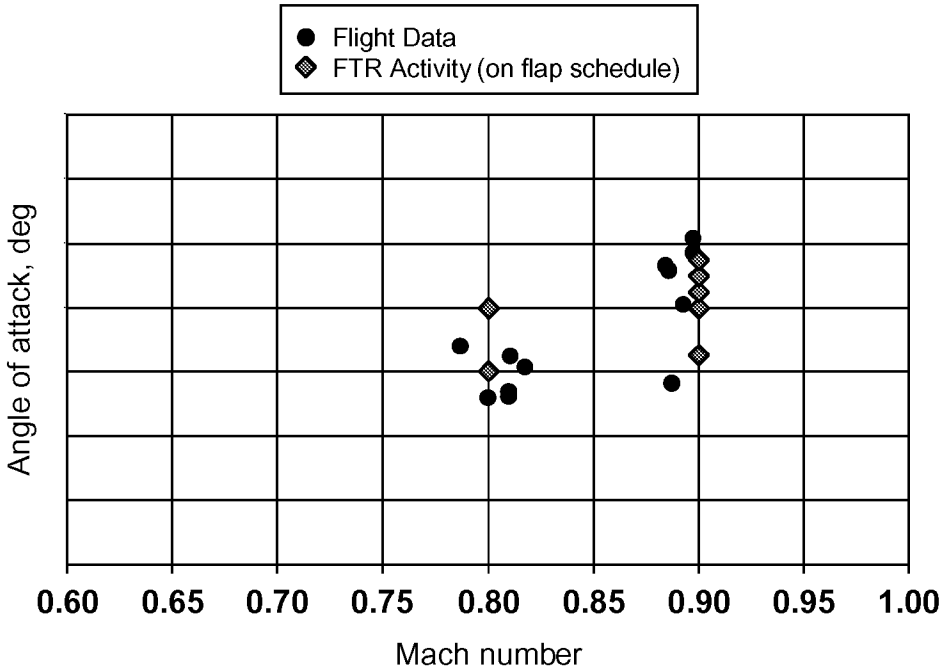

Figure 36. Comparison of free-to-roll and flight data for
the pre-production F/A-18E.

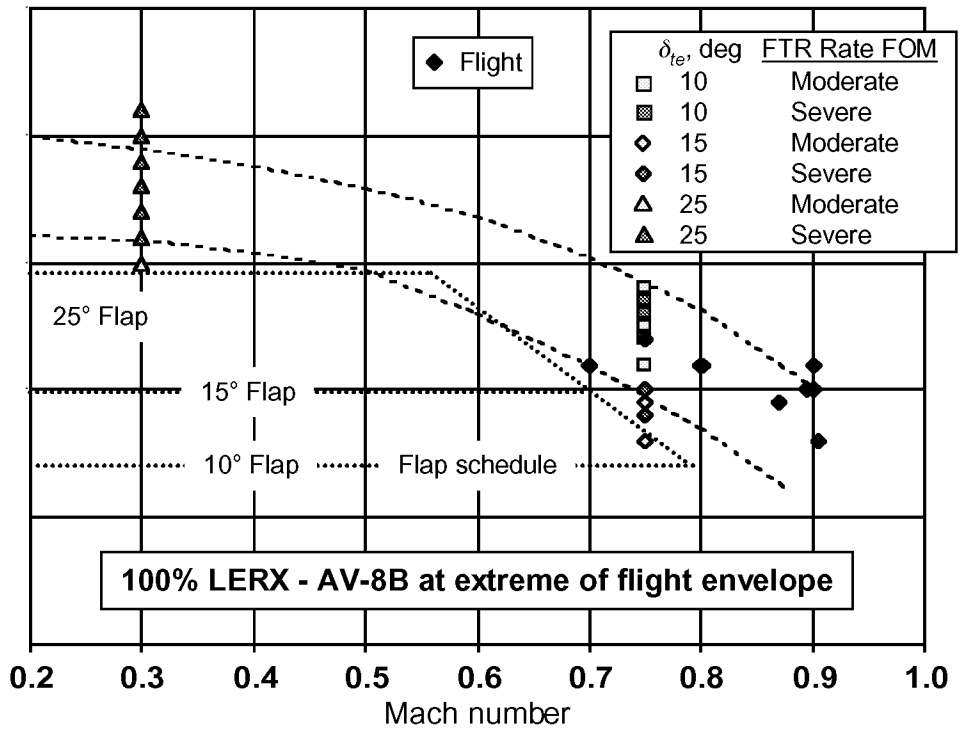

Figure 37. Comparison of free-to-roll and flight data for the AV-8B, 100% LERX.

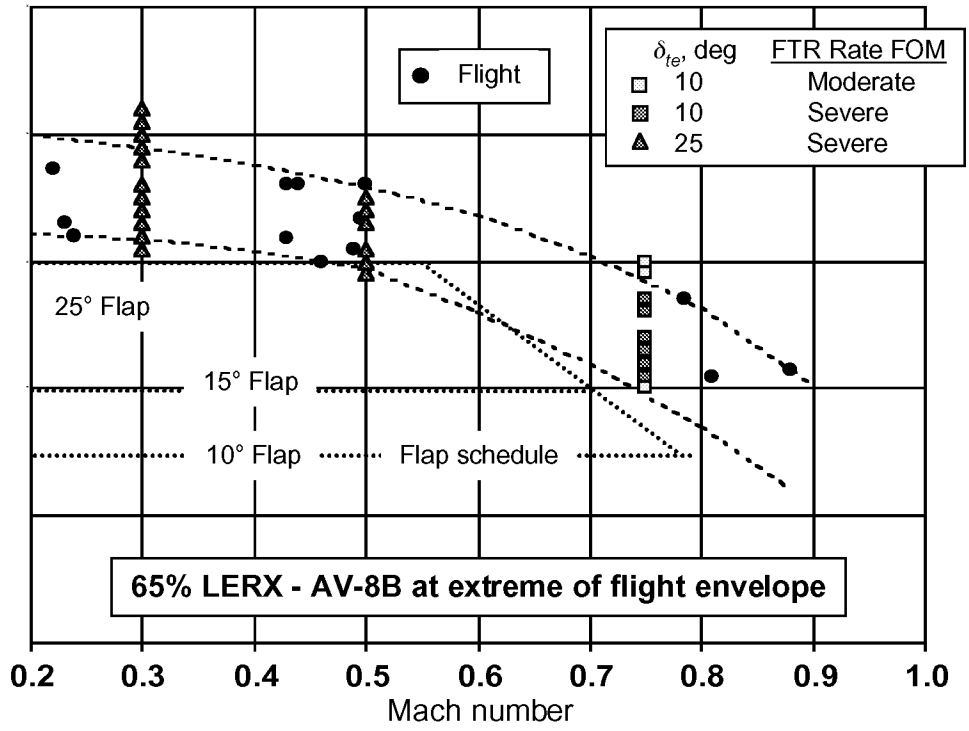

Figure 38. Comparison of free-to-roll and flight data for the AV-8B, 65% LERX.

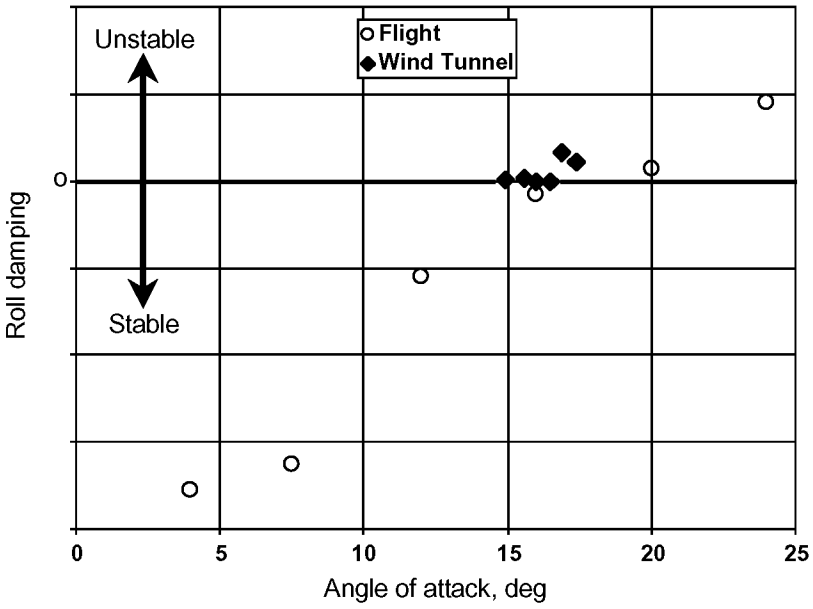

Figure 38. Comparison of free-to-roll and flight roll damping for the AV-8B.